Targeting methionine synthase in a fungal pathogen causes a metabolic imbalance that impacts cell energetics, growth and virulence

Jennifer Scott[1], Monica Sueiro-Olivares[1], Benjamin P. Thornton[2], Rebecca A. Owens[3], Howbeer Muhamadali[4], Rachael Fortune-Grant[1], Darren Thomson[1], Riba Thomas[1], Katherine Hollywood[5], Sean Doyle[3], Royston Goodacre[4], Lydia Tabernero[2], Elaine Bignell[1+] and Jorge Amich[1]*

Running Title: Fungal methionine synthase in vivo target validation

1. Manchester Fungal Infection Group (MFIG), Division of Infection, Immunity and Respiratory Medicine, School of Biological Sciences, Faculty of Biology, Medicine and Health, University of Manchester, Manchester Academic Health Science Centre, Manchester, UK.
2. School of Biological Sciences, Faculty of Biology, Medicine and Health, University of Manchester, Manchester Academic Health Science Centre, Manchester, UK.
3. Department of Biology, Maynooth University, Co. Kildare, Ireland.
4. Department of Biochemistry, Institute of Integrative Biology, University of Liverpool, Liverpool, UK.
5. Manchester Institute of Biotechnology. University of Manchester, Manchester, UK.

+Current address: Medical Research Council Centre for Medical Mycology, School of Biosciences, University of Exeter, Exeter, United Kingdom.

*Corresponding author: jorge.amichelias@manchester.ac.uk

ABSTRACT

There is an urgent need to develop novel antifungals to tackle the threat fungal pathogens pose to human health. In this work, we have performed a comprehensive characterisation and validation of the promising target methionine synthase (MetH). We uncover that in *Aspergillus fumigatus* the absence of this enzymatic activity triggers a metabolic imbalance that causes a reduction in intracellular ATP, which prevents fungal growth even in the presence of methionine. Interestingly, growth can be recovered in the presence of certain metabolites, which evidences that *metH* is a conditionally essential gene. As this implies that for a correct validation MetH should be targeted in established infections, we have validated the use of the tetOFF genetic model for fungal research and optimised its performance to mimic treatment of established infections. We show that repression of *metH* in growing hyphae halts growth *in vitro*, which translates into a beneficial effect when targeting established infections using this model *in vivo*. Finally, a structural-based virtual screening of methionine synthases reveals key differences between the human and fungal structures and unravels features in the fungal enzyme that can guide the design of novel specific inhibitors. Therefore, methionine synthase is a valuable target for the development of new antifungals.

IMPORTANCE

Fungal pathogens are responsible for millions of life-threatening infections on an annual basis worldwide. The current repertoire of antifungal drugs is very limited and, worryingly, resistance has emerged and already become a serious threat to our capacity to treat fungal diseases. The first step to develop new drugs often is to identify molecular targets which inhibition during infection can prevent pathogen growth. However, the current models are not suitable to validate targets in established infections. Here we have characterised the promising antifungal target methionine synthase in great detail, using the prominent fungal pathogen *Aspergillus fumigatus* as a model. We have uncovered the underlying reason for its essentiality and confirmed its druggability. Furthermore, we have optimised the use of a genetic system to show a beneficial effect of targeting methionine synthase in established infections. Therefore, we believe that antifungal drugs to target methionine synthase should be pursued and additionally, we propose that antifungal targets should be validated in a model of established infection.

63 **INTRODUCTION**

64 Fungal pathogens represent an increasing risk to human health (1), with over one billion people
65 worldwide affected by mycoses annually. Many of these mycoses are superficial infections of
66 the skin, nails or mucosal membranes and although troublesome are usually not life-
67 threatening. However, some fungi cause devastating chronic and invasive fungal infections,
68 which result in an estimated 1.6 million deaths per year (2). Incidences of invasive infections
69 caused by *Aspergillus*, *Candida*, *Cryptococcus* and *Pneumocystis* species are increasing (3), a
70 cause for serious concern as these genera are responsible for 90% of deaths caused by mycoses
71 (4). Despite the availability of antifungal drugs, mortality rates for invasive aspergillosis, invasive
72 candidiasis, cryptococcal meningitis and *Pneumocystis jirovecii* pneumonia are intolerably high,
73 reaching over 80%, 40%, 50% and 30% respectively (2, 5). There are currently only four classes
74 of antifungals in clinical use to treat invasive infections (azoles, echinocandins, polyenes and
75 flucytosine), all suffering from pharmacological drawbacks including toxicity, drug-drug
76 interactions and poor bioavailability (6, 7). With the sole exemption of flucytosine, which is only
77 used in combinatory therapy with amphotericin B for cryptococcal meningitis and *Candida*
78 endocarditis (7), the current antifungals target critical components of the fungal cell membrane
79 or cell wall (8), which represents a very limited druggable space. The rise of antifungal resistance
80 presents an additional challenge as mortality rates in patients with resistant isolates can reach
81 100%, making the development of new antifungal drugs increasingly critical for human health
82 (1, 9). Targeting fungal primary metabolism is broadly considered a valid strategy for the
83 development of novel antifungals, as it is crucial for pathogen virulence and survival (10, 11). A
84 primary example of success of this strategy is olorofim (F901318), a novel class of antifungal that
85 targets the pyrimidine biosynthesis pathway (12), which is currently in clinical trials.

86 Methionine synthases catalyse the transfer of a methyl group from *N*5-methyl-5,6,7,8-
87 tetrahydrofolate (CH_3-THF) to L-homocysteine (Hcy). Two unrelated protein families catalyse
88 this reaction: cobalamin dependent methionine synthases (EC 2.1.1.13) and cobalamin
89 independent methionine synthases (EC 2.1.1.14). Members of both families must catalyse the
90 transfer of a low active methyl group from the tertiary amine, CH_3-THF, to a relatively weak
91 nucleophile, Hcy sulfur. Cobalamin dependent enzymes facilitate this transfer by using
92 cobalamin as an intermediate methyl carrier (13). By contrast, cobalamin independent enzymes
93 directly transfer the methyl group from CH_3-THF to Hcy (14). Logically, proteins of each family
94 differ significantly both at amino acid sequence (15) and 3D structure level (16).

95 We have previously shown that the methionine synthase-encoding gene is essential for *A.*
96 *fumigatus* viability and virulence, which led us to propose it as a promising target for antifungal

97 drug development (17). In support of this, a systematic metabolic network analysis by Kaltdorf
98 and colleagues identified methionine synthase as a promising antifungal drug target worthy of
99 investigation (11). Methionine synthase has also been described as essential for *Candida*
100 *albicans* viability (18, 19) and necessary for *Cryptococcus neoformans* pathogenicity (20), which
101 suggests that a drug developed against this enzyme may have a broad spectrum of action.
102 Moreover, fungal methionine synthases are cobalamin independent, differing significantly from
103 the cobalamin dependent human protein at the amino acid sequence level: only 11.2% identity,
104 20.4% similarity and 60.2% gaps when aligned the *A. fumigatus* and human proteins using L-
105 Align from EMBL (21, 22). Therefore, it should be possible to develop drugs with low toxicity
106 potential.

107 Target validation is critical and has been suggested as the most important step in translating
108 a new potential target into a viable drug target because of its role in achieving efficacy in patients
109 (23). Indeed a retrospective analysis from AstraZeneca's drug pipeline showed that projects that
110 had performed a more thorough target validation were less likely to fail: 73% of the projects
111 were active or successful in Phase II compared with only 43% of projects without such extra
112 target validation (24). Therefore, in this work we aimed to further substantiate methionine
113 synthase's potential as an antifungal drug target, before advancing the drug discovery process.
114 In particular, we were interested in 1) unravelling the mechanistic basis of methionine synthase
115 essentiality in *A. fumigatus*, which is needed to fully explore the potential of this enzyme as drug
116 target and to be able to anticipate drug resistance mechanisms; and 2) developing *in vivo* models
117 of infection to mimic treatment against the target in an established infection and using them to
118 validate methionine synthase as an antifungal drug target.

119

120 **RESULTS AND DISCUSSION**

121 *Methionine synthase enzymatic activity is essential for Aspergillus fumigatus viability*

122 We had previously demonstrated that the methionine synthase encoding gene is essential for
123 *A. fumigatus* viability and virulence (17); however, the underlying reason for this essentiality was
124 still unclear. To address this question, here we have constructed strains that express the *metH*
125 gene under the control of a tetOFF system recently adapted for *Aspergillus* (25) in two different
126 *A. fumigatus* wild-type backgrounds, ATCC46645 and A1160. The advantage of the tetOFF
127 system over other regulatable systems is that doxycycline (Dox) can be added to downregulate
128 gene expression in growing hyphae (Fig. S1A), and thus this system permits investigation of the
129 consequences of the repression of an essential gene in growing mycelia. The constructed

130 *metH_tetOFF* strains (*H_OFF*) grew as the wild type in the absence of Dox, but as little as 0.5
131 µg/mL was sufficient to completely prevent colony development on an agar plate even in the
132 presence of methionine (Fig. S1B). This corroborates our previous result that methionine
133 synthase is essential for *A. fumigatus* viability and that its absence does not result in a sheer
134 auxotrophy for methionine (17).

135 Methionine synthase forms an interjection between the trans-sulfuration pathway and the
136 one carbon metabolic route (Fig. 1A), as the enzyme utilizes 5-methyl-tetrahydrofolate as co-
137 substrate. Therefore, the essentiality of *metH* might be due to required integrities of the trans-
138 sulfuration pathway or of the one carbon metabolic route. Alternatively, it could be that the
139 presence of the enzyme itself is essential, either because its enzymatic activity is required or
140 because it is fulfilling an unrelated additional role, as being part of a multiprotein complex. To
141 start discerning among these possibilities, we constructed a double *ΔmetGΔcysD* mutant,
142 blocked in the previous step of the trans-sulfuration pathway, and a *ΔmetF* deletant, which
143 blocks the previous step of the one-carbon metabolic route (Fig. 1A). As we had previously
144 observed (26), to rescue fully *ΔmetF*'s growth the media had to be supplemented with
145 methionine and other amino acids, as the folate cycle is necessary for the interconversion of
146 serine and glycine and plays a role in histidine and aromatic amino acid metabolism (27, 28).
147 Consequently, we added a mix of all amino acids except cysteine and methionine to the S-free
148 medium for this experiment. Phenotypic tests (Fig. 1B) confirmed that the *ΔmetGΔcysD* and
149 *ΔmetF* mutants were viable and could grow in the presence of methionine. In contrast, the
150 *H_OFF* conditional strain could not grow under restrictive conditions even in the presence of the
151 amino acid mix and methionine (Fig. 1B). Therefore, the MetH protein itself, and not the integrity
152 of the trans-sulfuration and one-carbon pathways, is essential for *A. fumigatus* viability.
153 Interestingly, the methionine auxotroph *ΔmetGΔcysD* was avirulent in a leukopenic model of
154 pulmonary aspergillosis (Fig. S1C), suggesting that the amount of readily available methionine
155 in the lung is very limited, not sufficient to rescue its auxotrophy. Indeed, the level of methionine
156 in human serum was calculated to be as low as ~20 µM (29, 30), which was described as
157 insufficient to support the growth of various auxotrophic bacterial pathogens (31) and we have
158 also observed that is not enough to rescue growth of the *A. fumigatus ΔmetGΔcysD* auxotroph.

159 Essentiality of the MetH protein could be directly linked to its enzymatic activity or,
160 alternatively, the protein could be performing an additional independent function. To discern
161 between these two possibilities, we constructed two strains that express single-point mutated
162 versions of MetH from the innocuous Ku70 locus of the *H_OFF* background strain, under the
163 control of its native promoter (Fig. 1C). These point mutations, $metH^{g2042A>2C}$ (D616A) and

164 *metH*$^{g2179TA>9GC}$ (Y662A), were previously described to prevent conformational rearrangements
165 required for activity of the *C. albicans* methionine synthase (32). In the absence of Dox, these
166 strains grew normally, as they expressed both the wild-type MetH, from the tetOFF promoter,
167 and the mutated version of the protein (Fig. 1C). In the presence of Dox, when the wild-type
168 *metH* gene was downregulated, the Y662A strain grew on sulfate worse than in non-restrictive
169 conditions, but still to a significant extent, suggesting that this point mutation did not completely
170 abrogate enzymatic activity (Fig. 1C). Interestingly, Y662 grew normally on methionine, showing
171 that methionine can compensate for a partial reduction of MetH activity (Fig 1C). The D616A
172 mutated protein was confirmed to be stable as a GFP-tagged version of this protein could be
173 visualised in -Dox conditions (Fig. S1D, strain detailed later in the manuscript). Interestingly, the
174 D616A strain (two isolates were tested) was not able to grow on sulfate (Fig. 1C), demonstrating
175 that enzymatic activity was fully blocked. Nor could it grow on methionine (Fig. 1C), indicating
176 that enzymatic activity is required for viability even in the presence of the full protein. All these
177 phenotypes support the conclusion that methionine synthase enzymatic activity is required for
178 viability.

179

180 *Absence of methionine synthase enzymatic activity results in a shortage of crucial metabolites,*
181 *but does not cause toxic accumulation of homocysteine*

182 The absence of methionine synthase enzymatic activity has two direct consequences, which
183 could cause deleterious effects and therefore explain its essentiality (Fig. 1A). It could cause an
184 accumulation of the potentially toxic substrate homocysteine and/or a shortage of the co-
185 product tetrahydrofolate (THF). THF is directly converted to 5,10-methylene-THF, which is
186 required for the synthesis of purines and thymidylate (TMP), and thus for DNA synthesis;
187 additionally, as purine biosynthesis requires Gln, Gly and Asp, and THF *de novo* synthesis
188 requires chorismate (precursor of aromatic amino acids), a shortage of THF might cause a
189 depletion of amino acids (Fig. 1A). To investigate if the depletion of any of these metabolites
190 underlies MetH essentiality, we supplemented the media with a number of precursors and
191 potentially depleted metabolites (Fig. 2A). Added as sole supplement, only adenine was able to
192 trigger growth, but to a minimal degree. Further addition of a mixture of all amino acids
193 noticeably improved growth. Supplementation with adenine and guanine (purine bases) did also
194 reconstitute noticeable growth, which was not enhanced with further addition of amino acids.
195 Folic acid was also capable of reconstituting growth, but only when amino acids were added as
196 the sole N-source (Fig. S3). However, no combination of compounds was able to reconstitute
197 growth to the wild-type level. This suggests that a shortage of relevant metabolites derived from

198 THF, prominently adenine, partially accounts for methionine synthase essentiality, but cannot
199 explain it completely. In other fungi, as *Pichia pastoris* (33) or *Schizosaccharomyces pombe* (34),
200 summplementation with methionine and adenine was found to restore growth of a *metH*
201 mutant to wild-type levels, denoting them as combined auxotrophs. In *A. fumigatus* it seems to
202 be more complex because supplementation with methionine, adenine and other amino acids
203 could still not fully restore growth, suggesting that more factors are implicated.

204 To investigate if homocysteine could be accumulating to toxic levels in the absence of MetH
205 activity, we over-expressed several genes that should alleviate its accumulation. To this aim we
206 designed and constructed the plasmid pJA49, which allows direct integration of any ORF to
207 episomally overexpress genes in *A. fumigatus*. Plasmid pJA49 carries the *A. nidulans* AMA1
208 autologous replicating sequence (35, 36) and the hygromycin B resistance gene (*hygrB*) as a
209 selection marker. A unique *Stu*I restriction site allows introduction of any PCR amplified ORF in
210 frame under the control of the *A. fumigatus* strong promoter *hspA* (37) and the *A. nidulans trpC*
211 terminator (Fig S2A). Using this plasmid, we produced a strain in the *H_OFF* background that
212 episomally overexpresses *mecA,* encoding cystathionine-β-synthase, which converts
213 homocysteine to cystathionine (Fig. 1A). Homocysteine exerts toxic effects through its
214 conversion to *S*-adenosylhomocysteine, which causes DNA hypomethylation (38, 39), or to
215 homocysteine thiolactone, which causes *N*-homocysteinylation at the ε-amino group of protein
216 lysine residues (40, 41). Consequently, we also constructed strains that episomally over-express
217 genes that could detoxify those products: the *S*-adenosyl-homocysteinase lyase encoding gene
218 *sahL* (AFUA_1G10130) or the *A. nidulans* homocysteine thiolactone hydrolase encoding gene
219 *blhA* (AN6399) (*A. fumigatus* genome does not encode any orthologue) (Fig. S2B). However,
220 despite a strong over-expression of the genes (Fig. S2C&D), none of them could rescue growth
221 of the *H_OFF* strain in restrictive conditions (Fig. 2B). Therefore, our over-expression
222 experiments suggest that homocysteine accumulation is not responsible for *metH* essentiality,
223 but additional experiments such as quantification homocysteine levels, which are currently
224 challenging, would be required to further support this hypothesis. Addition of adenine to the
225 medium did not improve growth of the overexpression strains further than that of the *H_OFF*
226 background (Fig. 2B), indicating that methionine synthase essentiality seemingly is not a
227 combined effect of homocysteine accumulation and depletion of THF-derived metabolites. Toxic
228 accumulation of homocysteine was speculated to be the underlying reason of methionine
229 synthase essentiality in both *Candida albicans* and *Cryptococcus neoformans* (19, 20) but our
230 results suggest that this is not the case in *A. fumigatus*. Therefore, we propose that the previous
231 assumption should be revisited in other fungal pathogens.

232

233 *Methionine synthase repression triggers a metabolic imbalance that causes a decrease in cell*
234 *energetics*

235 Aiming to identify any adverse metabolic shift in the absence of MetH and/or accumulation of
236 toxic compounds that could explain its necessity for proper growth, we performed a
237 metabolomics analysis, via gas chromatography-mass spectrometry (GC-MS), comparing the
238 metabolites present in wild-type and *H_OFF* strains before and 6 h after Dox addition. Before
239 Dox addition both strains clustered closely together in a Principal Component Analysis (PCA)
240 scores plot (Fig. S4A), showing that their metabolic profiles are highly similar. However, 6 h after
241 Dox addition the strains clusters became clearly separated, denoting differential metabolite
242 content. Analysis of the differentially accumulated metabolites (full list can be consulted in Table
243 S1) using the online platforms MBRole (42) and Metaboanalyst (43, 44) did not reveal any
244 obvious metabolic switch, probably due to the rather small number of metabolites that could
245 be identified by cross-referencing with the Golm library (http://gmd.mpimp-golm.mpg.de/).
246 Manual inspection of the metabolites pointed out interesting aspects. Firstly, the methionine
247 levels were not significantly different, which demonstrates that methionine supplementation in
248 the growth medium triggers correct intracellular levels in the *H_OFF* strain; this undoubtedly
249 rules out that a shortage of methionine could be the cause of the essentiality of methionine
250 synthase. Secondly, we detected a significantly lower amount of adenosine in the *H_OFF* strain
251 compared with the wild-type after Dox addition (Fig. 3A), which is in agreement with our
252 previous result that supplementation of adenine can partially reconstitute growth in the
253 absence of MetH. We did not find accumulation of compounds with a clear toxic potential upon
254 *metH* repression. Nevertheless, we detected a lower amount of several amino acids (Phe, Ser,
255 Glu, Pro, Ile, Thr, Ala and Asp, Fig. S4B), which suggests that the cells may enter into growth
256 arrest upon *metH* repression. Interestingly, we noticed a significantly lower accumulation of
257 some metabolites of the glycolysis pathway and TCA cycle (Fig. 3A) and some other mono and
258 poly-saccharides (Fig. S4B). These variations could reflect a low energetic status of the cells upon
259 *metH* repression. Indeed, we found that the level of ATP significantly decreased in the *H_OFF*
260 strain, but not in the wild-type, upon Dox addition (Fig. 3B). Therefore, we evaluated if
261 supplementation of the medium with substrates that have the potential to increase cell
262 energetics can rescue *H_OFF* growth in restrictive conditions. We found that when pyruvate,
263 which can directly be converted to acetyl-CoA to enter the TCA cycle, was added as the sole
264 carbon source *H_OFF* growth was reconstituted in restrictive conditions to the same level as the
265 wild-type (Fig. 3C). Growth was limited for both strains, as pyruvate does not appear to be a

266 good carbon source (45). However, the presence of glucose in the medium precluded the
267 reconstitution of growth of *H_OFF* (Fig. S3), as it has been described to prevent pyruvate uptake
268 in *S. cerevisiae* (46). We next tested the capacity of ATP to be used an alternative energy source
269 and to reconstitute growth. To diversify the presence of permeases in the cell membrane, and
270 thus maximise the chance of ATP uptake, we assayed two different N-sources: ammonium (NH_4^+,
271 preferred source) and amino acids (Fig. S3). Indeed, when amino acids were the only N-source,
272 supplementation of the medium with ATP reconstituted *H_OFF* growth in restrictive conditions
273 to wild type levels (Fig. 3C). This agrees with the recent observation that eukaryotic cells can
274 uptake ATP and exploit it as an energy source (47). In conclusion, a decrease in cell energetics
275 developed in the absence of methionine synthase seems to explain MetH essentiality for
276 growth.

277 The fact that growth in the absence of methionine synthase can be reconstituted when there
278 are sufficient levels of methionine and ATP implies that *metH* is a conditionally essential gene,
279 meaning that it is only essential in the absence of the specific conditions that overcome the
280 disturbances derived from its deficiency. We believe that a significant number of genes
281 previously described as essential in fungi would in fact be conditionally essential, however the
282 right conditions to reconstitute growth have not been identified in many cases. This highlights a
283 paramount consideration for the proper identification and validation of drug targets: the
284 deficiencies introduced by targeting a conditionally essential gene must not be overcome during
285 infection. This important concept has already been discussed by others (48-51) and we believe
286 addressing it should become the standard for proper validation of antimicrobial targets. In the
287 case of methionine synthase, it is unlikely that the fungus could acquire sufficient levels of ATP
288 (combined with methionine and not using a preferred N-source) in the lung tissue to overcome
289 the growth defect resulting from targeting MetH. The concentration of free extracellular ATP in
290 human plasma has been calculated to be in the sub-micromolar range (28-64 nM) (52). In the
291 lungs, extracellular ATP concentrations must be strictly balanced and increased levels are
292 implicated in the pathophysiology of inflammatory diseases (53); nevertheless, even in such
293 cases ATP levels have been calculated in the low micromolar range (54, 55). Despite this low
294 concentrations and consequently unlikely compensation, we believe that MetH needs to be
295 validated in a suitable model to confirm that its deficiency cannot be not overcome in
296 established infections.

297 We then questioned how the lack of methionine synthase's enzymatic activity could cause a
298 drop in cell energy. We hypothesised that blockage of methionine synthase activity likely causes
299 a forced conversion of 5,10-methylene-THF to 5-methyl-THF by the action of MetF (Fig. 1A). In

300 support of this, we observed that expression of *metF* was increased in the *H_OFF* strain (Fig. 3D).
301 This likely causes a shortage of 5,10-methylene-THF, as the conversion is not reversible and THF
302 cannot be recycled by the action of methionine synthase (Fig. 1A). Indeed, supplementation of
303 folic acid (only when amino acids are the sole N-source, Fig. S3) and of purines could partially
304 restore growth (Fig. 2A), as they compensate for the deficit in purine ring biosynthesis when
305 there is a shortage of 5,10-methylene-THF. However, this still does not explain why there is a
306 drop in ATP. We hypothesised that the block of purine biosynthesis might be sensed as a
307 shortage of nucleotides. This could then cause a shift in glucose metabolism from glycolysis and
308 the TCA cycle (which produce energy) to the Pentose Phosphate Pathway (PPP), which is
309 required to produce ribose-5-phosphate, an integral part of nucleotides. In a similar vein, it has
310 recently been described that activation of anabolism in *Saccharomyces cerevisiae* implies
311 increased nucleotide biosynthesis and consequently metabolic flow through the PPP (56). To
312 evaluate our hypothesis, we investigated the transcription level of the glucose-6-phosphate
313 dehydrogenase (G6PD) encoding gene (AFUA_3G08470), which catalyses the first committed
314 step of the PPP. In agreement with our hypothesis, the expression of G6PD encoding gene
315 increases in the *H_OFF* strain upon addition of Dox (Fig. 3D), likely reflecting an increased flow
316 through the PPP. We then wondered how cells may be activating the PPP. The target of
317 rapamycin (TOR) TORC1 effector, which is widely known to activate anabolism and growth (57-
318 59), has been described to activate the PPP in mammalian cells (60, 61) and has been
319 functionally connected with energy production and nucleotide metabolism in *A. fumigatus* (62).
320 In addition, the cAMP/PKA (protein kinase A) pathway is known to be paramount for sensing of
321 nutrients and the correspondent adaptation of gene expression and metabolism (63), and was
322 found to be implicated in the regulation of nucleotide biosynthesis in *A. fumigatus* (64).
323 Consequently, we explored if a partial block of TOR with low concentrations of rapamycin or of
324 PKA with H-89 could prevent the imbalanced activation of the PPP in the absence of MetH
325 activity. However, neither of the inhibitors could reconstitute growth of the *H_OFF* strain in
326 restrictive conditions (Fig. S4C). This means that neither the TOR nor the PKA pathways seem to
327 be involved in the deleterious metabolic shift that seemingly activates PPP and decreases flux
328 through glycolysis. Therefore, more experiments are required to elucidate the mechanism
329 underlying the metabolic imbalance developed upon *metH* downregulation.

330 In summary, we propose that absence of methionine synthase activity causes a strong defect
331 in purine biosynthesis that the cell tries to compensate for by shifting carbon metabolism to the
332 PPP; this metabolic imbalance causes a drop of ATP levels, which collapses cell energetics and
333 results in halted growth (Fig. 3E).

334 Interestingly, we also detected that *metF* expression is higher in the *H_OFF* strain compared
335 to the wild-type, even in the absence of Dox (Fig. 3D). This could be explained as an effort to
336 compensate a higher demand of 5-methyl-THF by the slightly increased amount of methionine
337 synthase in this strain (Fig. S1A). This effect could cause a mild defect in purine biosynthesis in
338 the *H_OFF* strain, and indeed adenosine content was lower in the *H_OFF*–Dox condition
339 compared with the wild-type–Dox sample in the metabolome analysis (Fig 3A). Furthermore,
340 this also explains why we detected a small but significant increase of G6PD expression in the
341 *H_OFF*–Dox condition (Fig. 3D). Therefore, it seems that upregulating methionine synthase has
342 the potential to cause the same metabolic imbalance as downregulating it. However, the effect
343 of overexpression (notice that it is only ~1.5 fold in our strain Fig. S1A) is minor and does not
344 have obvious consequences for growth, as THF can be recycled and thus the shortage of 5,10-
345 methylene-THF is not severe. In any case, two important points can be highlighted from this
346 small imbalance. Firstly, methionine synthase activity is very important and must be finely tuned
347 to maintain a proper metabolic homeostasis. Secondly, changing the expression level of genes
348 with constitutive and/or regulatable promoters can have unexpected and hidden consequences
349 that often go unnoticed.

350

351 *Supplementation with S-adenosylmethionine reconstitutes ATP levels and growth*

352 We have shown that the absence of MetH activity causes a reduction in ATP levels. *S*-
353 adenosylmethionine (SAM) is produced from methionine and ATP by the action of *S*-
354 adenosylmethionine synthetase SasA (Fig. 1A), an essential enzyme in *A. nidulans* (65). Hence,
355 we reasoned that the absence of MetH activity might cause a decrease in SAM levels. To test
356 that hypothesis, we first attempted to rescue growth of the *H_OFF* strain in a medium
357 supplemented with methionine and SAM. We tested various N-sources to diversify the presence
358 of permeases in the cell membrane, aiming to maximise the chances of SAM uptake (Fig. S3).
359 Indeed, the addition of SAM reconstituted growth of the *H_OFF* strain in restrictive conditions
360 in the presence of methionine when amino acids were the only N-source (Fig. 4A and S3). We
361 then measured the intracellular concentration of SAM in growing mycelia upon addition of Dox
362 using MS/MS. Surprisingly, we observed that addition of Dox to the *H_OFF* strain did not cause
363 a significant reduction in SAM levels (Fig. 4B). Consequently, we wondered how the addition of
364 SAM may reconstitute *H_OFF* growth if its levels are not reduced upon *metH* repression. We
365 speculated that as SAM is a crucial molecule it continues to be produced even if the levels of
366 ATP are reduced, draining it from other cellular processes and thus triggering energy

367 deprivation. In support of this hypothesis, we observed that supplementing SAM to the medium
368 increased the levels of ATP in growing hyphae (Fig. 4C).

369 As SAM supplementation can reconstitute *H_OFF* growth, it constitutes another condition
370 that overcomes the conditional essentiality of *metH*, highlighting again the need to validate
371 MetH in a model of established infection. The concentration of SAM in human serum is
372 extremely low, in the range of 100-150 nM (30), and consequently it is unlikely that the fungus
373 could find sufficient SAM during infection to compensate for the defect in ATP caused by
374 targeting methionine synthase.

375 *S*-adenosylmethionine plays a fundamental role as methyl donor for the majority of cellular
376 methylation reactions, including methylation of DNA. Given the observed importance of SAM in
377 the absence of MetH activity and considering that in *P. pastoris* and *C. albicans* methionine
378 synthase was reported to localise in the nucleus, as well as in the cytoplasm (33), we speculated
379 that nuclear localization might be important for MetH cellular function. To test this hypothesis,
380 we constructed strains expressing different versions of C-terminus GFP-tagged MetH from the
381 pJA49 plasmid (Fig. S2) in the *H_OFF* background. These were a wild-type MetH, a $MetH^{D616A}$
382 (control of no growth –Fig. 1C & S5A–) and a $MetH^{R749A}$ (*metH*$^{g2439CG>GA}$) version of the protein,
383 which according to the results published for *P. pastoris* should not localise in the nucleus (33).
384 The strain expressing wild-type MetH grew normally in restrictive conditions (Fig. S5A), proving
385 that the tagged MetH-GFP protein was active. Importantly, this result also demonstrated that
386 genetic downregulation of *metH* is the only reason for the lack of growth of the *H_OFF* strain in
387 the presence of Dox. We confirmed that *A. fumigatus* MetH localises in both the nucleus and
388 cytoplasm (Fig 4D & S5B). In contrast to what was described in *P. pastoris*, the $MetH^{R749A}$ protein
389 seems to be active, as it could trigger growth of *H_OFF* in restrictive conditions (Fig. S5A) and
390 still localised into the nucleus (Fig. S5B). Therefore, the possibility that MetH localisation in the
391 nucleus is important needs further exploration.

392

393 *Repression of methionine synthase causes growth inhibition in growing mycelia*

394 The major advantage of the tetOFF system is that it can be employed to simulate a drug
395 treatment before a specific chemical is developed. Addition of Dox to a growing mycelium
396 downregulates the gene of interest (Fig S1A), mimicking the effect of blocking its product by the
397 action of a drug. The validity of the Tet systems has recently been questioned, as it has been
398 reported that Dox can impair mitochondrial function in various eukaryotic models (66).
399 Nevertheless, existing evidence suggests that low concentrations of Dox (≤ 50 µg/mL) have little

400 effect on fungal cells. For instance, in contrast to reports of Dox affecting proliferation of human
401 cells at low concentrations (66, 67), we and others have not detected negative effects of low
402 concentrations of Dox or of tetracycline on fungal proliferation (Fig. 5A), phenotype
403 (macroscopic or microscopic, Fig. 5B) or virulence (17, 68-74). In addition, it was reported that
404 40 µg/mL of Dox does not affect the transcriptional profile of *S. cerevisiae* (75), which contrasts
405 with the broad effect caused by only 1 µg/mL Dox on global transcription in human cells (66).
406 Moreover, a study that investigated the role of various mitochondrial proteins for its function in
407 *C. albicans* did not observe any negative effect of 20 µg/mL Dox on fungal growth nor on
408 mitochondrial morphology and function (76). To test the effect of Dox on *A. fumigatus*, we grew
409 the wild-type strain overnight in various concentrations of drug and imaged mitochondria using
410 the Rhodamine 123 dye (Fig S6). It was previously described that inhibition of translation in
411 mitochondrial (mechanism of Dox toxicity) promotes mitochondrial fission, which can be
412 detected as a more fragmented, punctuate, mitochondrial appearance compared to the healthy
413 tubular morphology (66, 76). This fragmented phenotype started to appear, although there was
414 variation among hyphae, when the fungus was incubated in 100 µg/mL Dox and became obvious
415 when it was incubated in 1000 µg/mL Dox (Fig. S6). In contrast, in low concentrations of Dox (1
416 and 10 µg/mL Dox) the mitochondria showed a healthy tubular morphology, indistinguishable
417 from that of no Dox (Fig. S6). Therefore, low concentrations of Dox do not affect mitochondria
418 morphology and thus likely do not impair their function. In fact, we have also observed that
419 addition of 5 µg/mL Dox to wild-type mycelium did not affect the ATP content (Fig 3B), further
420 supporting the conclusion that mitochondrial function is not impaired. Therefore, even if higher
421 concentrations of Dox have a negative effect on fungal cells (70, 74), its impact at low
422 concentrations on fungal cells seems to be minimal. Consequently, we argue that as long as the
423 concentration of Dox used is ≤ 50 µg/mL, the tetOFF system can be utilised to investigate the
424 consequences of downregulating gene expression in fungal research.

425 To investigate the effect of downregulating *metH* for mycelial growth, we added Dox to 12,
426 16 or 24 h grown submerged mycelia and left it incubating for an additional 24 h. Addition of
427 Dox to 12 or 16 h grown mycelia severely impaired growth of the *H_OFF* strain but not the wt,
428 as observed by biomass (Fig. 5A) and OD (Fig. S7A) measurements. This effect was lost when
429 Dox was added to 24 h grown mycelia, due to the incapacity of Dox to reach and downregulate
430 expression in all cells within the dense mass of an overgrown mycelium. Interestingly, Dox
431 addition to methionine free media stopped *H_OFF* growth immediately, which can be observed
432 by comparing fungal biomass at the time of Dox addition to the measurement 24 h after Dox
433 addition. In contrast, the fungus inoculated in methionine containing media grew a little further

434 after Dox addition (Fig. 5A). To understand this difference, we added Dox to either resting or 8
435 h germinated conidia and imaged them 16 and 40 h after drug addition (Fig. 5B & Fig. S7B). In
436 agreement with the previous result, we observed that Dox addition in methionine free medium
437 inhibited growth immediately: resting conidia did not germinate and germinated conidia did not
438 elongate the germtube. In contrast, after addition of Dox in methionine containing medium,
439 most of the resting conidia were still able to germinate and some germlings could elongate the
440 germinated tubes to form short hyphae. This suggests that the drop in ATP levels takes ~3-4 h
441 before having an effect on growth. Importantly, once growth was inhibited, the effect was
442 sustained for a long period, as we could not detect further growth up to 40 h post-inoculation.
443 To corroborate these observations and further determine whether the effect of growth is
444 fungistatic or fungicidal in the long term, we performed a time-lapse analysis of the effects of
445 adding Dox to 8 h swollen conidia and its subsequent withdrawal after 16 h of incubation (Fig.
446 5C and Video 1). We observed that growth was inhibited ~4 h after Dox addition and almost
447 completely halted after 6 h, which was sustained as long as the drug was present. Upon
448 withdrawal of Dox, growth resumes within 6 h (Fig 5D and Video S1), showing that the effect of
449 blocking MetH is fungistatic, at least with the genetic TeOFF model of *metH* repression. As
450 expected Dox had no effect on wild-type growth (Video S2).

451

452 *Targeting MetH in established infections interferes with the progression of disease*

453 We previously used the TetON system to investigate the relevance of MetH in *A. fumigatus*
454 virulence (17). In this model, *metH* gene expression was active when mice were fed with Dox,
455 which resulted in full virulence of the *metH_tetON* strain (demonstrating that the concentration
456 of Dox reached in murine tissues does not impact fungal virulence). In the absence of Dox the
457 gene was not expressed, which completely abrogated virulence. This proved that the murine
458 lung does not readily provide the conditions to overcome the conditional essentiality of *metH*,
459 and thus this gene is required to establish infection. However, antifungal drugs are normally
460 administered to treat patients who already have an established infection. Therefore, it is
461 possible that the conditional essentiality of the gene could be overcome when the fungus is
462 actively growing in the tissue, as the fungal metabolic requirements and the environmental
463 conditions are different (49, 50). Consequently, in order to achieve a rigorous target validation,
464 it is crucial to assess the efficiency of new target candidates in established infections. The first
465 conditional promoter system used for *A. fumigatus in vivo* was the (p)niiA (48). This system
466 represses genetic expression of the gene of interest in the presence of ammonium, which is
467 contained in murine serum. Accordingly, in this seminal study several genes essential *in vitro*

468 were confirmed or refuted to be essential to initiate infection in a model of systemic (blood)
469 infection. Currently, two more systems are in use to assess the relevance of fungal essential
470 genes for pulmonary infection: TetON and (p)xylP. These systems can be used to either impede
471 or permit fungal gene expression in murine lungs; but in both models this control can only be
472 exerted from the beginning of infection, as sufficient levels of the inducing molecule
473 (doxycycline or xylose) must be present to activate gene expression in the control condition.
474 Consequently, these models have been used to investigate the relevance of genes required to
475 grow *in vitro* to initiate pulmonary infection (17, 72, 77). However, those models cannot be used
476 to determine the importance of the genes in established aspergillosis infections *in vivo*.
477 Therefore, we aimed to optimise the use of the TetOFF system for this purpose, as it can be used
478 to downregulate gene expression in growing mycelia. As a control for the model, we constructed
479 a *cyp51A_tetOFFΔcyp51B* (*51A_OFF*) strain. We reasoned that the target of the azoles, first-line
480 treatment drugs for *Aspergillus* diseases, should be the gold standard to compare any target
481 against. This strain showed a similar behaviour as *H_OFF in vitro*: as little as 0.05 µg/ml Dox
482 prevented colony development on an agar plate (Fig. S8A) and addition of Dox to conidia or
483 germlings blocked growth (Fig. S8B).

484 We first assayed the use of the TetOFF system in the *Galleria mellonella* alternative mini-host
485 model of infection. Preliminary experiments revealed that the balance between reaching
486 sufficient levels of Dox to exert an effect and maintaining toxic effects of overdose low was very
487 delicate. We finally optimised a regimen consisting of 5 injections of 50 mg/kg Dox (Fig. S9A)
488 that caused little mortality in the control group (25% in Dox control VS 12% in PBS treatment
489 control P=0.22) but still showed an effect of treatment (Fig. 6A). We then infected *Galleria* larvae
490 with 5×10^2 conidia of *51A_OFF* or *H_OFF* strains and applied the Dox regimen or PBS vehicle
491 starting at the same time of infection (0 h) or 6 h after infection (Fig. S9A). For both strains,
492 administration of Dox from the beginning of infection triggered a significant improvement in
493 survival compared with the non-treated conditions (50% VS 17.2% for *51A_OFF*, P=0.0036, and
494 41.45% VS 6.67% for *H_OFF*, P=0.022) (Fig. 6A). The fact that administration of Dox at the time
495 of infection did not improve survival to close to 100%, was not surprising, as it is important to
496 note that Dox does not completely prevent gene expression (Fig. S1A), so a moderate effect on
497 survival was expectable. Furthermore, rapid metabolization of the drug in the larvae hemocoel
498 or microenvironment variations in its concentration may also account for a discrete effect of
499 treatment. Despite this limitations of the model, we observed that administration of Dox 6 h
500 after infection also triggered a significant improvement in survival for both strains (42.8% VS
501 17.2% for *51A_OFF*, P=0.0007, and 32.26% VS 6.67% for *H_OFF*, P=0.0324) (Fig. 6A). Therefore,

502 downregulation of methionine synthase genetic expression in established infections conferred
503 a significant benefit in survival which was comparable to that observed with the target of the
504 azoles.

505 The positive results obtained using the *Galleria* infection model prompted us to assay the
506 TetOFF system in a leukopenic murine model of pulmonary aspergillosis. To ensure that Dox
507 levels in mouse lungs reach and maintain sufficient concentrations to downregulate gene
508 expression (according to our results *in vitro*) we performed a pilot Dox dosage experiment in
509 immunosuppressed non-infected mice (Fig S8B). We extracted lungs of Dox treated mice at
510 different time-points, homogenated them and measured Dox concentration using a bioassay
511 based on inhibition of *Escherichia coli DH5α* growth. We could detect promising levels of Dox in
512 all mice (concentrations ranging from 2.2 to 0.94 µg/mL –Fig. S9B–) which according to our
513 results *in vitro* should be sufficient to downregulate gene expression from the TetOFF system.
514 We therefore infected leukopenic mice with 10^5 spores of the *51A_OFF* or the *H_OFF* strains and
515 administered PBS vehicle or our Dox regimen, starting 16 h after infection (Fig. S9B). The use of
516 an uninfected, Dox treated control group uncovered that the intense Dox regimen used was
517 harmful for the mice. These uninfected mice lost weight at a similar rate as the infected groups
518 and looked ill from the third or fourth day of treatment. This is not surprising as Dox can impair
519 mitochondrial function in mice (66) and has iron chelating properties (78). As a consequence,
520 there was no beneficial effect of Dox treatment on survival (not shown). The fact that Dox
521 treatment did also not show any benefit in survival for our control strain *51A_OFF*, which should
522 mimic treatment with azoles (primary therapy for invasive aspergillosis), indicates that the
523 TetOFF system is not ideal to mimic a drug treatment in established infections. Nevertheless, we
524 further attempted to determine the efficiency of targeting MetH in established infections by
525 measuring fungal burdens in lungs of treated and untreated mice. We observed that two and a
526 half days of Dox treatment (when the mice have not developed visible toxic effects yet) did result
527 in a significant reduction of fungal burdens 3 days after infection for both *51A_OFF* (P=0.0279)
528 and *H_OFF* (P=0.0019) (Fig. 6B). Therefore, we could observe a beneficial effect of interfering
529 with methionine synthase genetic expression in an established pulmonary infection, which was
530 comparable to that of interfering with the expression of *cyp51A*, the target of azoles. This
531 constitutes a very rigorous validation of MetH as a promising antifungal target.

532 A recent study also aimed to use another TetOFF system to validate a drug target in
533 established aspergillosis infections (79). These authors administered Dox exclusively through
534 oral gavage, accounting for lower dosage of drug. Consequently, even if no toxic effect for the
535 mice was observed, they also did not detect any beneficial effect on survival when the Dox

536 treatment was initiated after infection. Therefore, the TetOFF system is clearly not optimal and
537 better models are needed. Yet, it is currently the only model with which the efficiency of new
538 targets can be tested in aspergillosis established infections, and thus it is highly valuable that we
539 have been able to optimise its use *in vivo*. Our *51A_OFF* control strain has been key to calibrating
540 the model, and allows us to be confident that the beneficial effects observed, even if subtle, are
541 significant. Hence, we propose that hereinafter proper genetic validation of antifungal targets
542 should include testing their relevance in established infections.

543

544 *Structural-based virtual screening of MetH*

545 Having shown *in vivo* that MetH is a promising target, we decided to investigate its druggability
546 by running a structural-based virtual screening. The sequence of *A. fumigatus* MetH (AfMetH)
547 contains two predicted methionine synthase domains with a β-barrel fold conserved in other
548 fungal and bacterial enzymes. The structure of the *C. albicans* orthologue (80) (CaMetH) showed
549 that the active site is located between the two domains where the methyl tetrahydrofolate, the
550 homocysteine substrate and the catalytic zinc ion bind in close proximity. The homology model
551 for AfMetH (Fig. 7A) overlaps very well with that of the CaMetH thus providing a suitable
552 molecular model for further analysis. In contrast, the structure of the human methionine
553 synthase (hMS) shows a very different overall arrangement with the folate and homocysteine
554 binding domains located in completely different regions (Fig. 7B). Comparison of the
555 tetrahydrofolate binding sites between the fungal and the human structures also highlights
556 significant structural differences that affect the conformation adopted by the ligand. In the
557 CaMetH structure the 5-methyl-tetrahydrofolate (C2F) adopts a bent conformation (<20Å long)
558 and it is in close proximity to the methionine product, whereas in the human structure the
559 tetrahydrofolate (THF) ligand binds in an elongated conformation extending up to 30Å from end
560 to end, (Fig. 7 C&D).

561 Virtual screening (VS) was carried on the AfMetH and the hMS structures with the Maybridge
562 Ro3 fragment library to explore potential venues for drug development. The results showed four
563 ligand binding clusters in the AfMetH structure, two of which (C1, C2) match the binding position
564 of the 5-methyl-tetrahydrafolate and the methionine from the CaMetH crystal structure (Fig.
565 7E). For the hMS, we found two main clusters, C1 that overlaps with the tetrahydrofolate binding
566 site and C2 in a nearby pocket. Clearly the distribution of the clusters defines a very different
567 landscape around the folate site between the human and the fungal enzymes. Furthermore, the
568 proximity of the C1 and C2 clusters, matching the folate and Met/homocysteine binding sites in

569 the Ca/Af proteins means that it may be possible to combine ligands at both sites to generate
570 double-site inhibitors with high specificity towards the fungal enzymes. Antifolates are a class of
571 drugs that antagonise folate, blocking the action of folate dependent enzymes such as
572 dihydrofolate reductase (DHFR), thymidylate synthase or methionine synthase. Methotrexate is
573 an antifolate commonly used to treat cancer and autoimmune diseases. Interestingly,
574 methotrexate has been shown to be a weak inhibitor of the *C. albicans* methionine synthase
575 (32) and to have some antifungal activity against *C. albicans* (81) and *Aspergillus ssp* (82).
576 Nevertheless, methotrexate is not a good antifungal drug, as its activity is high against human
577 enzymes (IC_{50} of 0.3 µM for DHFR (83)) and low against fungal methionine synthase (IC_{50} of 4
578 mM for *C. albicans* MetH (32)). Therefore, more potent and specific inhibitors of fungal
579 methionine synthases are needed to fully exploit the value of this target for antifungal therapy,
580 a task that seems possible and can be directed from our analyses.

581

582 In summary, we have shown that methionine synthase blockage triggers not only methionine
583 auxotrophy, but also a metabolic imbalance that results in a drop in cellular energetics and
584 growth arrest. In light of our results, we stress that conditional essentiality is important to
585 understand the underlying mechanisms of metabolic processes and needs to be considered to
586 achieve proper validation of novel antimicrobial targets. Accordingly, we proved that targeting
587 methionine synthase in established infections has a beneficial effect similar to that observed for
588 the target of azoles, the most effective drugs for the treatment of aspergillosis. Finally, we
589 showed that fungal methionine synthases have distinct druggable pockets that can be exploited
590 to design specific inhibitors. In conclusion, we have demonstrated that fungal methionine
591 synthases are promising targets for the development of novel antifungals.

592

593

594 **MATERIAL AND METHODS**

595 *Strains, media and culture conditions*

596 The *Escherichia coli* strain DH5α (84) was used for cloning procedures. Plasmid-carrying *E. coli*
597 strains were routinely grown at 37°C in LB liquid medium (Oxoid) under selective conditions (100
598 $\mu g \cdot mL^{-1}$ ampicillin or 50 $\mu g \cdot mL^{-1}$ kanamycin); for growth on plates, 1.5% agar was added to
599 solidify the medium. All plasmids used in the course of this study were generated using the
600 Seamless Cloning (Invitrogen) technology as previously described (17, 85). *E. coli* strain BL21

601 (DE3) (86) was grown on Mueller Hinton agar (Sigma) in bioassays, to determine Dox
602 concentrations within homogenized murine lungs.

603 The wild-type clinical isolate *Aspergillus fumigatus* strain ATCC 46645 served as reference
604 recipient. *A. fumigatus* strain A1160 (*ku80Δ*) (87) was also used to confirm *metH* essentiality. *A.*
605 *fumigatus* mutants were generated using a standard protoplasting protocol (88). *A. fumigatus*
606 strains were generally cultured in minimal medium (MM) (89) (1% glucose, 5 mM ammonium
607 tartrate, 7 mM KCl, 11 mM KH_2PO_4, 0.25 mM $MgSO_4$, 1× Hutner's trace elements solution; pH
608 5.5; 1.5% agar) at 37°C. For selection in the presence of resistance markers 50 $\mu g \cdot mL^{-1}$ of
609 hygromycin B or 100 $\mu g \cdot mL^{-1}$ of pyrithiamine (InvivoGen) were applied. In sulfur-free medium
610 (MM-S), $MgCl_2$ substituted for $MgSO_4$ and a modified mixture of trace elements lacking any
611 sulfate salt was used. For all growth assays on solid media, the culture medium was inoculated
612 with 10 µl of a freshly prepared *A. fumigatus* spore suspension (10^5 conidia$\cdot mL^{-1}$ in water
613 supplemented with 0.9% NaCl and 0.02% Tween 80) and incubated at 37°C for 3 days.

614 *Extraction and manipulation of nucleic acids*

615 Standard protocols of recombinant DNA technology were carried out (90). Phusion® high-fidelity
616 DNA polymerase (ThermoFisher Scientific) was generally used in polymerase chain reactions and
617 essential cloning steps were verified by sequencing. Fungal genomic DNA was prepared
618 following the protocol of Kolar *et al.* (91) and Southern analyses were carried out as described
619 (92, 93), using the Amersham ECL Direct Labeling and Detection System® (GE Healthcare). Fungal
620 RNA was isolated using TRIzol reagent (ThermoFisher Scientific) and Qiagen plant RNA extraction
621 kit. Retrotranscription was performed using SuperScript III First-Strand Synthesis (ThermoFisher
622 Scientific). RT-PCR on both gDNA and cDNA was performed using the SYBR® Green JumpStart
623 (Sigma) in a 7500 Fast Real Time PCR cycler from Applied Biosystems.

624 *Microscopy*

625 10^3 *A. fumigatus* resting or 8 h germinated conidia were inoculated in 200 µL of medium (+/-
626 Dox) in 8 well imaging chambers (ibidi) and incubated at 37°C. Microscopy images were taken
627 on a Nikon Eclipse TE2000-E, using a CFI Plan Apochromat Lambda 20X/0.75 objective and
628 captured with a Hamamatsu Orca-ER CCD camera (Hamamatsu Photonics) and manipulated
629 using NIS-Elements 4.0 (Nikon). For extensively grown mycelia a stereomicroscope Leica MZFL-
630 III was used, with a Q-imaging Retinga 6000 camera, and manipulated using Metamorph v7760.
631 Confocal imaging was performed using a Leica TCS SP8x inverted confocal microscope equipped
632 with a 40X/0.85 objective. Nuclei were stained with DAPI (Life Technologies Ltd) as described

633 previously (94). GFP was excited at 458 nm with an Argon laser at 20% power. DAPI was excited
634 at 405 nm with an LED diode at 20%.

635 *Metabolome analyses*

636 *A. fumigatus* wild-type and *metH_tetOFF* strains were incubated in MM for 16 h before the -Dox
637 samples were taken (8 replicates of 11 mL each). Then, 5 µg/mL Dox and 5 mM methionine (to
638 prevent metabolic adaptation due to met auxotrophy) were added as appropriate and the
639 cultures incubated for 6 h, after which the +Dox samples were taken (8 × 11 mL). The samples
640 were immediately quenched with 2× volumes of 60% methanol at -48°C. After centrifugation at
641 4800 *g* for 10 min at -8°C, metabolites were extracted in 1 mL 80% methanol at -48°C by three
642 cycles of N_2 liquid snap freezing, thawing and vortexing. Supernatant was cleared by
643 centrifugation at -9 °C, 14,500 *g* for 5 min. Quality control (QC) samples were prepared by
644 combining 100 µL from each sample. Samples were aliquoted (300 µL), followed by the addition
645 of 100 µL of the internal standard solution (0.2 mg/mL succinic-d_4 acid, and 0.2 mg/mL glycine-
646 *d*5) and vortex mix for 15 s. All samples were lyophilised by speed vacuum concentration at room
647 temperature overnight (HETO VR MAXI vacuum centrifuge attached to a Thermo Svart RVT 4104
648 refrigerated vapour trap; Thermo Life Sciences, Basingstoke, U.K.). A two-step derivatization
649 protocol of methoxyamination followed by trimethylsilylation was employed (95).

650 GC-MS analysis was conducted on a 7890B GC coupled to a 5975 series MSD quadrupole
651 mass spectrometer and equipped with a 7693 autosampler (Agilent, Technologies, UK). The
652 sample (1 µL) was injected onto a VF5-MS column (30 m x 0.25 mm x 0.25 µm; Agilent
653 Technologies) with an inlet temperature of 280 °C and a split ratio of 20:1. Helium was used as
654 the carrier gas with a flow rate of 1 mL/min. The chromatography was programmed to begin at
655 70 °C with a hold time of 4 min, followed by an increase to 300 °C at a rate of 14 °C/min and a
656 final hold time of 4 min before returning to 70 °C. The total run time for the analysis was 24.43
657 min. The MS was equipped with an electron impact ion source using 70 eV ionisation and a fixed
658 emission of 35 µA. The mass spectrum was collected for the range 50-550 m/z with a scan speed
659 of 3,125 (*N*=1). Samples were analysed in a randomised order with the injection of a pooled
660 biological quality control sample after every 6th sample injection.

661 For data analysis, the GC-MS raw files were converted to mzXML and subsequently imported
662 to R. The R package "erah" was employed to de-convolve the GC-MS files. Chromatographic
663 peaks and mass spectra were cross-referenced with the Golm library for putative identification
664 purposes, and followed the metabolomics standards initiative (MSI) guidelines for metabolite
665 identification (96). The peak intensities were normalised according to the IS (succinic-d_4 acid)

666 before being log_{10}-scaled for further statistical analysis. All pre-processed data were investigated
667 by employing principal component analysis (PCA) (97).

668 The raw data of this metabolome analysis has been deposited in the MetaboLights database
669 (98), under the reference MTBLS1636 (www.ebi.ac.uk/metabolights/MTBLS1636)

670 *ATP Quantitation*

671 *A. fumigatus* was grown as in the metabolome analysis. However, where the effect of SAM was
672 investigated spores were inoculated into MM-N + 1mg/mL aac and 0.5mM SAM was also added
673 at the time of Dox addition. ATP levels were determined using the BacTiter-Glo™ Assay
674 (Promega) following the manufacturer's instructions and a TriStar LB 941 Microplate Reader
675 (Berthold).

676 *Isolation and detection of SAM*

677 *A. fumigatus* was grown exactly in the same conditions as described for the metabolome
678 analysis. Harvested mycelia were snap-frozen in liquid N_2 and stored at -70 °C before SAM
679 isolation. SAM extraction was carried out according to Owens *et al* (99). Briefly, frozen mycelia
680 were ground in liquid N_2 and 0.1 M HCl (250 µL) was added to ground mycelia (100 mg). Samples
681 were stored on ice for 1 h, with sample vortexing at regular intervals. Samples were centrifuged
682 at 13,000 *g* for 10 min (4 °C) to remove cell debris and supernatants were collected.
683 Concentration of protein in supernatants was determined using a Biorad Bradford protein assay
684 relative to a bovine serum albumin (BSA) standard curve. Clarified supernatants were adjusted
685 to 15 % (w/v) trichloroacetic acid to remove protein. After 20 min incubation on ice,
686 centrifugation was repeated and clarified supernatants were diluted with 0.1 % (v/v) formic acid.
687 Samples were injected onto a Hypersil Gold aQ C18 column with polar endcapping on a Dionex
688 UltiMate 3000 nanoRSLC with a Thermo Q-Exactive mass spectrometer. Samples were loaded in
689 100 % Solvent A (0.1 % (v/v) formic acid in water) followed by a gradient to 20 % B (Solvent B:
690 0.1 % (v/v) formic acid in acetonitrile) over 4 min. Resolution set to 70000 for MS, with MS/MS
691 scans collected using a Top3 method. SAM standard (Sigma) was used to determine retention
692 time and to confirm MS/MS fragmentation pattern for identification. Extracted ion
693 chromatograms were generated at m/z 399-400 and the peak area of SAM was measured.
694 Measurements were taken from three biological and two technical replicates per sample,
695 normalized to the protein concentration in the extracts from each replicate. SAM levels are
696 expressed as a percentage relative to the parental strain in the absence of Dox.

697 *Nuclei isolation and Western Blot*

698 Protoplasts were generated as in *A. fumigatus* transformations and nuclei isolated were isolated
699 by sucrose gradient fractionation as previously described by Sperling and Grunstein (100).
700 Nuclear localisation of GFP-tagged target proteins was confirmed by Western-blot. Aliquots of
701 nuclei were boiled for 5 minutes in loading buffer (0.2 M Tris-HCl, 0.4 M DTT, 8% SDS, trace
702 bromophenol blue) and separated on a 12% (w/v) SDS-PAGE gel. The proteins were transferred
703 to a Polyvinylidene difluoride (PVDF) membrane using the Trans-Blot® Turbo™ Transfer System
704 (Bio-Rad). Detection of GFP was carried out with a rabbit polyclonal anti-GFP antiserum (Bio-
705 Rad) and anti-rabbit IgG HRP-linked antibody (Cell Signalling Technology). SuperSignal West Pico
706 PLUS Chemiluminescent Substrate (Thermo Scientific) and the ChemiDoc XRS+ Imaging System
707 (Biorad) were used to visualise immunoreactive bands. Ponceau S staining was performed to
708 normalize the Western-blot signal to the protein loading.

709 *Mitochondria imaging*

710 Approximately 200 *A. fumigatus* spores were seeded onto Ibidi 8-well slides in minimal medium
711 containing 0, 1, 10, 100 and 1000 µg/ml Dox and incubated at 37 °C for 16 hours. The culture
712 medium was then replaced with minimal medium containing the same Dox concentrations plus
713 10 µM Rhodamine 123 dye and further incubated for 1-2 hours at 37 °C prior to live-cell confocal
714 imaging. High-resolution confocal fluorescence imaging was performed at 37 °C on a Leica SP8x
715 using a 63x/1.3NA oil immersion lens, whereby Rhodamine 123 fluorescence was excited with a
716 white light laser (5%) tuned to 508 nm and the emission collected on HyD detectors set to 513-
717 600 nm. Representative single plane images of each condition were background-subtracted
718 (rolling ball 20 pixel radius) in Fiji (101) and montaged using FigureJ (102).

719 *Biomass measurement*

720 Conidia were inoculated into MM-S, supplemented with either methionine or sulfate, and
721 incubated at 37°C 180 rpm for 12, 16 or 24 h. After this initial incubation, 3 mL samples were
722 taken in triplicate from the cultures, filtered through tared Miracloth, dried at 60°C for 16 h and
723 their biomass measured. In treated conditions Dox was added to a final concentration of 1
724 µg/mL and the culture allowed to grow for a further 24 h at 37°C 180 rpm. 5 mL samples were
725 taken in triplicate and their biomass measured as above.

726 *Galleria mellonella infections*

727 Sixth-stage instar larval *G. mellonella* moths (15 to 25 mm in length) were ordered from the Live
728 Foods Company (Sheffield, United Kingdom). Infections were performed according to Kavanagh
729 and Fallon (103). Randomly selected groups of 15 larvae were injected in the last left proleg with

730 10 µL of a suspension of 5×10^4 conidia/mL in PBS, using Braun Omnican 50-U 100 0.5- mL insulin
731 syringes with integrated needles. Dox was administered according to the treatment shown in
732 Fig. S9A, alternating injections in the last right and left prolegs. In each experiment an untouched
733 and a saline injected control were included, to verify that mortality was not due to the health
734 status of the larvae or the injection method. Three independent experiments were carried out.
735 The presented survival curves display the pooled data, which was analysed with the Log-Rank
736 test.

737 *Ethics Statement*

738 All mouse experiments were performed under United Kingdom Home Office project license
739 PDF8402B7 and approved by the University of Manchester Ethics Committee and by the
740 Biological Services Facility at the Faculty of Biology, Medicine and Health, University of
741 Manchester.

742 *Leukopenic murine model of invasive pulmonary aspergillosis and calculation of fungal burden.*

743 Outbred CD1 male mice (22– 26 g) were purchased from Charles Rivers and left to rest for at
744 least 1 week before the experiment. Mice were allowed access *ad libitum* to water and food
745 throughout the experiment. Mice were immunosuppressed with 150 mg/kg of
746 cyclophosphamide on days -3 and -1 and with 250 mg/kg cortisone acetate on day -1. On day 0
747 mice were anesthetized with isofluorane and intranasally infected with a dose of 10^5 conidia (40
748 µL of a freshly harvested spore solution of 2.5×10^6 conidia/mL). Dox was administered
749 according to the treatment shown in Fig. S9B. Dox containing food was purchased from Envingo
750 (Safe-diet U8200 Version 0115 A03 0.625 g/kg Doxycycline Hyclate pellets). At the selected time-
751 point (72 h after infection for fungal burden) mice were sacrificed by a lethal injection of
752 pentobarbital, the lungs harvested and immediately frozen.

753 Frozen lungs were lyophilised for 48 h in a CoolSafe ScanVac freeze drier connected to a
754 VacuuBrand pump and subsequently ground in the presence of liquid nitrogen. DNA was
755 isolated from the powder using the DNeasy Blood & Tissue Kit (Qiagen). DNA concentration and
756 quality were measured using a NanoDrop 2000 (ThermoFisher Scientific). To detect the fungal
757 burden, 500 ng of DNA extracted from each infected lung were subjected to qPCR. Primers used
758 to amplify the *A. fumigatus* β-tubulin gene (AFUA_7G00250) were forward, 5'-
759 ACTTCCGCAATGGACGTTAC-3', and reverse, 5'- GGATGTTGTTGGGAATCCAC-3'. Those designed
760 to amplify the murine actin locus (NM_007393) were forward, 5'-CGAGCACAGCTTCTTTGCAG-3'
761 and reverse, 5'-CCCATGGTGTCCGTTCTGA-3'. Standard curves were calculated using different
762 concentrations of fungal and murine gDNA pure template. Negative controls containing no

763 template DNA were subjected to the same procedure to exclude or detect any possible
764 contamination. Three technical replicates were prepared for each lung sample. qPCRs were
765 performed using the 7500 Fast Real-Time PCR system (Thermo Fisher Scientific) with the
766 following thermal cycling parameters: 94 °C for 2 min and 40 cycles of 94°C for 15 s and 59°C for
767 1 min. The fungal burden was calculated by normalising the number of fungal genome
768 equivalents (i.e. number of copies of the tubulin gene) to the murine genome equivalents in the
769 sample (i.e number of copies of the actin gene) (104). Two independent experiments were
770 carried out (*n*=9, 5 mice in the first and 4 mice in the second experiment). Burdens for each
771 strain were compared using a Mann Whitney test.

772 *Molecular homology models and virtual screening*

773 The full-length sequence for AFUA_4G07360, the cobalamin-independent methionine synthase
774 MetH from *A. fumigatus* (AfMetH) was obtained from FungiDB (https://fungidb.org/fungidb)
775 (105). This sequence together with the structure of the *C. albicans* orthologue (CaMetH) (PDB
776 ID: 4L65, DOI: 10.1016/j.jmb.2014.02.006) were used to create the molecular homology model
777 in Modeller (version 9.23) (106) with the basic option mode. The AfMetH model was then used
778 for virtual screening with the semi-automated pipeline VSpipe (107). For comparison we also
779 performed virtual screening with the structure of the human methionine synthase (hMS)
780 containing the folate and homocysteine binding domains (PDB ID: 4CCZ). Docking was done
781 using the Maybridge Ro3 1000 fragment library with AutoDock Vina (108). Results were
782 inspected graphically using PyMol (v1.8.0.3 Enhanced for Mac OS X (Schrödinger). All images
783 were produced with PyMol.

784

785

786 **ACKNOWLDGEMENTS**

787 We acknowledge the use of the Phenotyping Center at Manchester (PCAM) for the use of their
788 microscopes and advanced image analysis workstations. We are grateful to Prof Sven
789 Krappmann for critical reading of the manuscript and his constant support and guidance. We
790 also are indebted to Prof Robert Cramer for his insightful feedback on the manuscript and
791 personal support. We would like to thank all members of MFIG for constant help and
792 encouragement.

793 JA was supported by a MRC Career Development Award (MR/N008707/1). JS was supported by
794 a BSAC scholarship (bsac-2016-0049). BPT was supported by a MRC Doctoral Training
795 Partnership PhD studentship. Q-Exactive mass spectrometer and nanoLC instrumentation were

796 funded by a competitive infrastructure award from Science Foundation Ireland (SFI)
797 (12/RI/2346(3)).

798 **AUTHOR CONTRIBUTION**

799 JS performed the majority of experiments, analysed and interpreted most of the data and
800 participated in the design of the project. MS helped with the acquisition and analysis of most of
801 the experiments. BT run the structural-based virtual screening. RAO measured SAM levels in
802 mycelia. HMA performed the metabolomic experiment, analysed and with RG interpreted the
803 data. RFG assisted with the mouse models of infection. DT performed the microscopy of *A.*
804 *fumigatus* mitochondria and supported the other microscopy experiments. RT helped with the
805 execution of qPCRs. KH helped to set up the GC-MS instrument. SD designed the MS/MS analysis
806 of SAM. RG designed the metabolome analysis and interpreted the data. LT designed the virtual
807 screening analysis and interpreted the data. EB participated in the design and conception of the
808 project. JA conceived and designed the project and analysed most of the data.

809 **COMPETING INTERESTS**

810 The authors declare no competing interests.

811 **DATA AVAILABILITY**

812 The raw data that support the findings of this study are available upon reasonable request to
813 the authors. The raw data of metabolome analysis has been deposited in the MetaboLights
814 database [85], under the reference MTBLS1636 (www.ebi.ac.uk/metabolights/MTBLS1636).

815

816

817

818

819

820

821

822

823

824

825 **REFERENCES**

826 1. Fisher MC, Hawkins NJ, Sanglard D, Gurr SJ. 2018. Worldwide emergence of resistance
827 to antifungal drugs challenges human health and food security. Science 360:739-742.
828 2. Bongomin F, Gago S, Oladele RO, Denning DW. 2017. Global and Multi-National
829 Prevalence of Fungal Diseases-Estimate Precision. J Fungi (Basel) 3.
830 3. Bitar D, Lortholary O, Le Strat Y, Nicolau J, Coignard B, Tattevin P, Che D, Dromer F.
831 2014. Population-based analysis of invasive fungal infections, France, 2001-2010.
832 Emerg Infect Dis 20:1149-55.
833 4. Brown GD, Denning DW, Gow NA, Levitz SM, Netea MG, White TC. 2012. Hidden
834 killers: human fungal infections. Sci Transl Med 4:165rv13.
835 5. Nyazika TK, Hagen F, Machiridza T, Kutepa M, Masanganise F, Hendrickx M, Boekhout
836 T, Magombei-Majinjiwa T, Siziba N, Chin'ombe N, Mateveke K, Meis JF, Robertson VJ.
837 2016. *Cryptococcus neoformans* population diversity and clinical outcomes of HIV-
838 associated cryptococcal meningitis patients in Zimbabwe. J Med Microbiol 65:1281-
839 1288.
840 6. Patterson TF, Thompson GR, 3rd, Denning DW, Fishman JA, Hadley S, Herbrecht R,
841 Kontoyiannis DP, Marr KA, Morrison VA, Nguyen MH, Segal BH, Steinbach WJ, Stevens
842 DA, Walsh TJ, Wingard JR, Young JA, Bennett JE. 2016. Executive Summary: Practice
843 Guidelines for the Diagnosis and Management of Aspergillosis: 2016 Update by the
844 Infectious Diseases Society of America. Clin Infect Dis 63:433-42.
845 7. Pound MW, Townsend ML, Dimondi V, Wilson D, Drew RH. 2011. Overview of
846 treatment options for invasive fungal infections. Med Mycol 49:561-80.
847 8. Ghannoum MA, Rice LB. 1999. Antifungal agents: mode of action, mechanisms of
848 resistance, and correlation of these mechanisms with bacterial resistance. Clin
849 Microbiol Rev 12:501-17.
850 9. Verweij PE, Chowdhary A, Melchers WJ, Meis JF. 2016. Azole Resistance in *Aspergillus*
851 *fumigatus*: Can We Retain the Clinical Use of Mold-Active Antifungal Azoles? Clin Infect
852 Dis 62:362-8.
853 10. Amich J, Krappmann S. 2012. Deciphering metabolic traits of the fungal pathogen
854 *Aspergillus fumigatus*: redundancy vs. essentiality. Frontiers in Microbiology Fungi and
855 Their Interactions.
856 11. Kaltdorf M, Srivastava M, Gupta SK, Liang C, Binder J, Dietl AM, Meir Z, Haas H,
857 Osherov N, Krappmann S, Dandekar T. 2016. Systematic Identification of Anti-Fungal
858 Drug Targets by a Metabolic Network Approach. Front Mol Biosci 3:22.
859 12. Oliver JD, Sibley GEM, Beckmann N, Dobb KS, Slater MJ, McEntee L, du Pre S,
860 Livermore J, Bromley MJ, Wiederhold NP, Hope WW, Kennedy AJ, Law D, Birch M.
861 2016. F901318 represents a novel class of antifungal drug that inhibits dihydroorotate
862 dehydrogenase. Proc Natl Acad Sci U S A 113:12809-12814.
863 13. Evans JC, Huddler DP, Hilgers MT, Romanchuk G, Matthews RG, Ludwig ML. 2004.
864 Structures of the N-terminal modules imply large domain motions during catalysis by
865 methionine synthase. Proceedings of the National Academy of Sciences of the United
866 States of America 101:3729-3736.
867 14. Peariso K, Zhou ZHS, Smith AE, Matthews RG, Penner-Hahn JE. 2001. Characterization
868 of the zinc sites in cobalamin-independent and cobalamin-dependent methionine
869 synthase using zinc and selenium X-ray absorption spectroscopy. Biochemistry 40:987-
870 993.
871 15. Gonzalez JC, Banerjee RV, Huang S, Sumner JS, Matthews RG. 1992. Comparison of
872 cobalamin-independent and cobalamin-dependent methionine synthases from
873 *Escherichia coli:* two solutions to the same chemical problem. Biochemistry 31:6045-
874 56.

875 16. Matthews RG, Smith AE, Zhou ZHS, Taurog RE, Bandarian V, Evans JC, Ludwig M. 2003.
876 Cobalamin-dependent and cobalamin-independent methionine synthases: Are there
877 two solutions to the same chemical problem? Helvetica Chimica Acta 86:3939-3954.
878 17. Amich J, Dumig M, O'Keeffe G, Binder J, Doyle S, Beilhack A, Krappmann S. 2016.
879 Exploration of Sulfur Assimilation of *Aspergillus fumigatus* Reveals Biosynthesis of
880 Sulfur-Containing Amino Acids as a Virulence Determinant. Infect Immun 84:917-29.
881 18. Segal ES, Gritsenko V, Levitan A, Yadav B, Dror N, Steenwyk JL, Silberberg Y, Mielich K,
882 Rokas A, Gow NAR, Kunze R, Sharan R, Berman J. 2018. Gene Essentiality Analyzed by
883 In Vivo Transposon Mutagenesis and Machine Learning in a Stable Haploid Isolate of
884 *Candida albicans*. MBio 9.
885 19. Suliman HS, Appling DR, Robertus JD. 2007. The gene for cobalamin-independent
886 methionine synthase is essential in *Candida albicans*: a potential antifungal target.
887 Arch Biochem Biophys 467:218-26.
888 20. Pascon RC, Ganous TM, Kingsbury JM, Cox GM, McCusker JH. 2004. *Cryptococcus*
889 *neoformans* methionine synthase: expression analysis and requirement for virulence.
890 Microbiology 150:3013-23.
891 21. Li W, Cowley A, Uludag M, Gur T, McWilliam H, Squizzato S, Park YM, Buso N, Lopez R.
892 2015. The EMBL-EBI bioinformatics web and programmatic tools framework. Nucleic
893 Acids Res 43:W580-4.
894 22. McWilliam H, Li W, Uludag M, Squizzato S, Park YM, Buso N, Cowley AP, Lopez R. 2013.
895 Analysis Tool Web Services from the EMBL-EBI. Nucleic Acids Res 41:W597-600.
896 23. Miwa GT. 2010. The Drug Discovery Process p1-14. *In* Lu C, Li AP (ed), Enzyme
897 Inhibition in Drug Discovery and Development: The Good and the Bad
898 doi:10.1002/9780470538951.
899 24. Cook D, Brown D, Alexander R, March R, Morgan P, Satterthwaite G, Pangalos MN.
900 2014. Lessons learned from the fate of AstraZeneca's drug pipeline: a five-dimensional
901 framework. Nature Reviews Drug Discovery 13:419-431.
902 25. Wanka F, Cairns T, Boecker S, Berens C, Happel A, Zheng X, Sun J, Krappmann S, Meyer
903 V. 2016. Tet-on, or Tet-off, that is the question: Advanced conditional gene expression
904 in *Aspergillus*. Fungal Genet Biol 89:72-83.
905 26. Scott J, Sueiro-Olivares M, Ahmed W, Heddergott C, Zhao C, Thomas R, Bromley M,
906 Latge JP, Krappmann S, Fowler S, Bignell E, Amich J. 2019. *Pseudomonas aeruginosa*-
907 Derived Volatile Sulfur Compounds Promote Distal *Aspergillus fumigatus* Growth and a
908 Synergistic Pathogen-Pathogen Interaction That Increases Pathogenicity in Co-
909 infection. Front Microbiol 10:2311.
910 27. Lucock M. 2000. Folic acid: nutritional biochemistry, molecular biology, and role in
911 disease processes. Mol Genet Metab 71:121-38.
912 28. Tzin V, Galili G. 2010. The Biosynthetic Pathways for Shikimate and Aromatic Amino
913 Acids in *Arabidopsis thaliana*. Arabidopsis Book 8:e0132.
914 29. Deakova Z, Durackova Z, Armstrong DW, Lehotay J. 2015. Two-dimensional high
915 performance liquid chromatography for determination of homocysteine, methionine
916 and cysteine enantiomers in human serum. J Chromatogr A 1408:118-24.
917 30. Elshorbagy AK, Jerneren F, Samocha-Bonet D, Refsum H, Heilbronn LK. 2016. Serum S-
918 adenosylmethionine, but not methionine, increases in response to overfeeding in
919 humans. Nutr Diabetes 6:e192.
920 31. Jochim A, Shi T, Belikova D, Schwarz S, Peschel A, Heilbronner S. 2019. Methionine
921 Limitation Impairs Pathogen Expansion and Biofilm Formation Capacity. Appl Environ
922 Microbiol 85.
923 32. Ubhi D, Kago G, Monzingo AF, Robertus JD. 2014. Structural analysis of a fungal
924 methionine synthase with substrates and inhibitors. J Mol Biol 426:1839-47.

925 33. Sahu U, Rajendra VKH, Kapnoor SS, Bhagavat R, Chandra N, Rangarajan PN. 2017.
926 Methionine synthase is localized to the nucleus in *Pichia pastoris* and *Candida albicans*
927 and to the cytoplasm in *Saccharomyces cerevisiae*. J Biol Chem 292:14730-14746.
928 34. Fujita Y, Ukena E, Iefuji H, Giga-Hama Y, Takegawa K. 2006. Homocysteine
929 accumulation causes a defect in purine biosynthesis: further characterization of
930 *Schizosaccharomyces pombe* methionine auxotrophs. Microbiology 152:397-404.
931 35. Gems D, Johnstone IL, Clutterbuck AJ. 1991. An autonomously replicating plasmid
932 transforms *Aspergillus nidulans* at high frequency. Gene 98:61-7.
933 36. Aleksenko AY, Clutterbuck AJ. 1995. Recombinational stability of replicating plasmids
934 in *Aspergillus nidulans* during transformation, vegetative growth and sexual
935 reproduction. Curr Genet 28:87-93.
936 37. Paul S, Klutts JS, Moye-Rowley WS. 2012. Analysis of promoter function in *Aspergillus*
937 *fumigatus*. Eukaryot Cell 11:1167-77.
938 38. Christopher SA, Melnyk S, James SJ, Kruger WD. 2002. S-adenosylhomocysteine, but
939 not homocysteine, is toxic to yeast lacking cystathionine beta-synthase. Mol Genet
940 Metab 75:335-43.
941 39. Perna AF, Ingrosso D, Lombardi C, Acanfora F, Satta E, Cesare CM, Violetti E, Romano
942 MM, De Santo NG. 2003. Possible mechanisms of homocysteine toxicity. Kidney Int
943 Suppl doi:10.1046/j.1523-1755.63.s84.33.x:S137-40.
944 40. Bretes E, Zimny J. 2013. Homocysteine thiolactone affects protein ubiquitination in
945 yeast. Acta Biochim Pol 60:485-8.
946 41. Jakubowski H. 2006. Pathophysiological consequences of homocysteine excess. J Nutr
947 136:1741S-1749S.
948 42. Lopez-Ibanez J, Pazos F, Chagoyen M. 2016. MBROLE 2.0-functional enrichment of
949 chemical compounds. Nucleic Acids Research 44:W201-W204.
950 43. Chong J, Soufan O, Li C, Caraus I, Li SZ, Bourque G, Wishart DS, Xia JG. 2018.
951 MetaboAnalyst 4.0: towards more transparent and integrative metabolomics analysis.
952 Nucleic Acids Research 46:W486-W494.
953 44. Xia JG, Psychogios N, Young N, Wishart DS. 2009. MetaboAnalyst: a web server for
954 metabolomic data analysis and interpretation. Nucleic Acids Research 37:W652-W660.
955 45. Fendt SM, Sauer U. 2010. Transcriptional regulation of respiration in yeast
956 metabolizing differently repressive carbon substrates. BMC Syst Biol 4:12.
957 46. Akita O, Nishimori C, Shimamoto T, Fujii T, Iefuji H. 2000. Transport of pyruvate in
958 *Saccharomyces cerevisiae* and cloning of the gene encoded pyruvate permease. Biosci
959 Biotechnol Biochem 64:980-4.
960 47. Forte GM, Davie E, Lie S, Franz-Wachtel M, Ovens AJ, Wang T, Oakhill JS, Macek B,
961 Hagan IM, Petersen J. 2019. Import of extracellular ATP in yeast and man modulates
962 AMPK and TORC1 signalling. J Cell Sci 132.
963 48. Hu W, Sillaots S, Lemieux S, Davison J, Kauffman S, Breton A, Linteau A, Xin C, Bowman
964 J, Becker J, Jiang B, Roemer T. 2007. Essential gene identification and drug target
965 prioritization in *Aspergillus fumigatus*. PLoS Pathog 3:e24.
966 49. Beattie SR, Mark KMK, Thammahong A, Ries LNA, Dhingra S, Caffrey-Carr AK, Cheng C,
967 Black CC, Bowyer P, Bromley MJ, Obar JJ, Goldman GH, Cramer RA. 2017. Filamentous
968 fungal carbon catabolite repression supports metabolic plasticity and stress responses
969 essential for disease progression. PLoS Pathog 13:e1006340.
970 50. Cramer RA. 2016. *In vivo* veritas: *Aspergillus fumigatus* proliferation and pathogenesis-
971 -conditionally speaking. Virulence 7:7-10.
972 51. Kowalski CH, Kerkaert JD, Liu KW, Bond MC, Hartmann R, Nadell CD, Stajich JE, Cramer
973 RA. 2019. Fungal biofilm morphology impacts hypoxia fitness and disease progression.
974 Nat Microbiol 4:2430-2441.
975 52. Gorman MW, Feigl EO, Buffington CW. 2007. Human plasma ATP concentration. Clin
976 Chem 53:318-25.

977 53. Ito S, Furuya K, Sokabe M, Hasegawa Y. 2016. Cellular ATP release in the lung and
978 airway. Aims Biophysics 3:571-584.
979 54. Mortaz E, Braber S, Nazary M, Givi ME, Nijkamp FP, Folkerts G. 2009. ATP in the
980 pathogenesis of lung emphysema. Eur J Pharmacol 619:92-6.
981 55. Riteau N, Gasse P, Fauconnier L, Gombault A, Couegnat M, Fick L, Kanellopoulos J,
982 Quesniaux VFJ, Marchand-Adam S, Crestani B, Ryffel B, Couillin I. 2010. Extracellular
983 ATP Is a Danger Signal Activating P2X(7) Receptor in Lung Inflammation and Fibrosis.
984 American Journal of Respiratory and Critical Care Medicine 182:774-783.
985 56. Walvekar AS, Srinivasan R, Gupta R, Laxman S. 2018. Methionine coordinates a
986 hierarchically organized anabolic program enabling proliferation. Mol Biol Cell
987 29:3183-3200.
988 57. De Virgilio C, Loewith R. 2006. The TOR signalling network from yeast to man. Int J
989 Biochem Cell Biol 38:1476-81.
990 58. Loewith R, Hall MN. 2011. Target of rapamycin (TOR) in nutrient signaling and growth
991 control. Genetics 189:1177-201.
992 59. Saxton RA, Sabatini DM. 2017. mTOR Signaling in Growth, Metabolism, and Disease.
993 Cell 168:960-976.
994 60. Thiepold AL, Lorenz NI, Foltyn M, Engel AL, Dive I, Urban H, Heller S, Bruns I, Hofmann
995 U, Drose S, Harter PN, Mittelbronn M, Steinbach JP, Ronellenfitsch MW. 2017.
996 Mammalian target of rapamycin complex 1 activation sensitizes human glioma cells to
997 hypoxia-induced cell death. Brain 140:2623-2638.
998 61. Tsouko E, Khan AS, White MA, Han JJ, Shi Y, Merchant FA, Sharpe MA, Xin L, Frigo DE.
999 2014. Regulation of the pentose phosphate pathway by an androgen receptor-mTOR-
1000 mediated mechanism and its role in prostate cancer cell growth. Oncogenesis 3:e103.
1001 62. Baldin C, Valiante V, Kruger T, Schafferer L, Haas H, Kniemeyer O, Brakhage AA. 2015.
1002 Comparative proteomics of a tor inducible *Aspergillus fumigatus* mutant reveals
1003 involvement of the Tor kinase in iron regulation. Proteomics 15:2230-43.
1004 63. Caza M, Kronstad JW. 2019. The cAMP/Protein Kinase a Pathway Regulates Virulence
1005 and Adaptation to Host Conditions in *Cryptococcus neoformans*. Front Cell Infect
1006 Microbiol 9:212.
1007 64. Grosse C, Heinekamp T, Kniemeyer O, Gehrke A, Brakhage AA. 2008. Protein kinase A
1008 regulates growth, sporulation, and pigment formation in *Aspergillus fumigatus*. Appl
1009 Environ Microbiol 74:4923-33.
1010 65. Gerke J, Bayram O, Braus GH. 2012. Fungal S-adenosylmethionine synthetase and the
1011 control of development and secondary metabolism in *Aspergillus nidulans*. Fungal
1012 Genet Biol 49:443-54.
1013 66. Moullan N, Mouchiroud L, Wang X, Ryu D, Williams EG, Mottis A, Jovaisaite V,
1014 Frochaux MV, Quiros PM, Deplancke B, Houtkooper RH, Auwerx J. 2015. Tetracyclines
1015 Disturb Mitochondrial Function across Eukaryotic Models: A Call for Caution in
1016 Biomedical Research. Cell Rep 10:1681-1691.
1017 67. Samant R, Ahler E, Sullivan WJ, Cass A, Braas D, York AG, Bensinger SJ, Graeber TG,
1018 Christofk HR. 2013. Doxycycline Alters Metabolism and Proliferation of Human Cell
1019 Lines. PLoS ONE 8.
1020 68. Sasse A, Hamer SN, Amich J, Binder J, Krappmann S. 2015. Mutant characterization and
1021 in vivo conditional repression identify aromatic amino acid biosynthesis to be essential
1022 for *Aspergillus fumigatus* virulence. Virulence 7:56-62.
1023 69. Binder J, Shadkchan Y, Osherov N, Krappmann S. 2020. The Essential Thioredoxin
1024 Reductase of the Human Pathogenic Mold *Aspergillus fumigatus* Is a Promising
1025 Antifungal Target. Frontiers in Microbiology 11.
1026 70. Miceli MH, Bernardo SM, Lee SA. 2009. In vitro analyses of the combination of high-
1027 dose doxycycline and antifungal agents against *Candida albicans* biofilms. International
1028 Journal of Antimicrobial Agents 34:326-332.

1029 71. Chen T, Wagner AS, Tams RN, Eyer JE, Kauffman SJ, Gann ER, Fernandez EJ, Reynolds
1030 TB, Heitman J. 2019. Lrg1 Regulates β (1,3)-Glucan Masking in *Candida albicans*
1031 through the Cek1 MAP Kinase Pathway. mBio 10.
1032 72. Stewart JIP, Fava VM, Kerkaert JD, Subramanian AS, Gravelat FN, Lehoux M, Howell PL,
1033 Cramer RA, Sheppard DC. 2020. Reducing *Aspergillus fumigatus* Virulence through
1034 Targeted Dysregulation of the Conidiation Pathway. mBio 11.
1035 73. Fiori A, Van Dijck P. 2012. Potent Synergistic Effect of Doxycycline with Fluconazole
1036 against *Candida albicans* Is Mediated by Interference with Iron Homeostasis.
1037 Antimicrobial Agents and Chemotherapy 56:3785-3796.
1038 74. Oliver BG, Silver PM, Marie C, Hoot SJ, Leyde SE, White TC. 2008. Tetracycline alters
1039 drug susceptibility in *Candida albicans* and other pathogenic fungi. Microbiology
1040 154:960-970.
1041 75. Wishart JA, Hayes A, Wardleworth L, Zhang N, Oliver SG. 2005. Doxycycline, the drug
1042 used to control thetet-regulatable promoter system, has no effect on global gene
1043 expression in *Saccharomyces cerevisiae*. Yeast 22:565-569.
1044 76. Xie JL, Bohovych I, Wong EOY, Lambert J-P, Gingras A-C, Khalimonchuk O, Cowen LE,
1045 Leach MD. 2017. Ydj1 governs fungal morphogenesis and stress response, and
1046 facilitates mitochondrial protein import via Mas1 and Mas2. Microbial Cell 4:342-361.
1047 77. Bauer I, Misslinger M, Shadkchan Y, Dietl AM, Petzer V, Orasch T, Abt B, Graessle S,
1048 Osherov N, Haas H. 2019. The Lysine Deacetylase RpdA Is Essential for Virulence in
1049 *Aspergillus fumigatus*. Front Microbiol 10:2773.
1050 78. Grenier D, Huot MP, Mayrand D. 2000. Iron-chelating activity of tetracyclines and its
1051 impact on the susceptibility of *Actinobacillus actinomycetemcomitans* to these
1052 antibiotics. Antimicrob Agents Chemother 44:763-6.
1053 79. Peng Y, Zhang H, Xu M, Tan MW. 2018. A Tet-Off gene expression system for validation
1054 of antifungal drug targets in a murine invasive pulmonary aspergillosis model. Sci Rep
1055 8:443.
1056 80. Ferrer JL, Ravanel S, Robert M, Dumas R. 2004. Crystal structures of cobalamin-
1057 independent methionine synthase complexed with zinc, homocysteine, and
1058 methyltetrahydrofolate. J Biol Chem 279:44235-8.
1059 81. Warnock DW, Johnson EM, Burke J, Pracharktam R. 1989. Effect of methotrexate alone
1060 and in combination with antifungal drugs on the growth of *Candida albicans*. J
1061 Antimicrob Chemother 23:837-47.
1062 82. Yang J, Gao L, Yu P, Kosgey JC, Jia L, Fang Y, Xiong J, Zhang F. 2019. In vitro synergy of
1063 azole antifungals and methotrexate against *Candida albicans*. Life Sci 235:116827.
1064 83. Fan CC, Vitols KS, Huennekens FM. 1980. Inhibition of dihydrofolate reductase by
1065 methotrexate: a new look at an old problem. Adv Enzyme Regul 18:41-52.
1066 84. Woodcock DM, Crowther PJ, Doherty J, Jefferson S, DeCruz E, Noyer-Weidner M, Smith
1067 SS, Michael MZ, Graham MW. 1989. Quantitative evaluation of *Escherichia coli* host
1068 strains for tolerance to cytosine methylation in plasmid and phage recombinants.
1069 Nucleic Acids Res 17:3469-78.
1070 85. Amich J, Schafferer L, Haas H, Krappmann S. 2013. Regulation of sulphur assimilation is
1071 essential for virulence and affects iron homeostasis of the human-pathogenic mould
1072 *Aspergillus fumigatus*. PLoS Pathog 9:e1003573.
1073 86. Wood WB. 1966. Host specificity of DNA produced by *Escherichia coli*: bacterial
1074 mutations affecting the restriction and modification of DNA. J Mol Biol 16:118-33.
1075 87. da Silva Ferreira ME, Kress MR, Savoldi M, Goldman MH, Hartl A, Heinekamp T,
1076 Brakhage AA, Goldman GH. 2006. The akuB(KU80) mutant deficient for
1077 nonhomologous end joining is a powerful tool for analyzing pathogenicity in
1078 *Aspergillus fumigatus*. Eukaryot Cell 5:207-11.

1079 88. Szewczyk E, Nayak T, Oakley CE, Edgerton H, Xiong Y, Taheri-Talesh N, Osmani SA,
1080 Oakley BR. 2006. Fusion PCR and gene targeting in *Aspergillus nidulans*. Nat Protoc
1081 1:3111-20.
1082 89. Kafer E. 1977. Meiotic and mitotic recombination in *Aspergillus* and its chromosomal
1083 aberrations. Adv Genet 19:33-131.
1084 90. Sambrook J, Fritsch EF, Maniatis T. 1989. Molecular Cloning: A Laboratory Manual, NY.
1085 91. Kolar M, Punt PJ, van den Hondel CA, Schwab H. 1988. Transformation of *Penicillium*
1086 *chrysogenum* using dominant selection markers and expression of an *Escherichia coli*
1087 *lacZ* fusion gene. Gene 62:127-34.
1088 92. Southern E. 2006. Southern blotting. Nat Protoc 1:518-25.
1089 93. Southern EM. 1975. Detection of specific sequences among DNA fragments separated
1090 by gel electrophoresis. J Mol Biol 98:503-17.
1091 94. Reverberi M, Punelli M, Smith CA, Zjalic S, Scarpari M, Scala V, Cardinali G, Aspite N,
1092 Pinzari F, Payne GA, Fabbri AA, Fanelli C. 2012. How peroxisomes affect aflatoxin
1093 biosynthesis in *Aspergillus flavus*. PLoS One 7:e48097.
1094 95. Wedge DC, Allwood JW, Dunn W, Vaughan AA, Simpson K, Brown M, Priest L, Blackhall
1095 FH, Whetton AD, Dive C, Goodacre R. 2011. Is Serum or Plasma More Appropriate for
1096 Intersubject Comparisons in Metabolomic Studies? An Assessment in Patients with
1097 Small-Cell Lung Cancer. Analytical Chemistry 83:6689-6697.
1098 96. Sumner LW, Amberg A, Barrett D, Beale MH, Beger R, Daykin CA, Fan TWM, Fiehn O,
1099 Goodacre R, Griffin JL, Hankemeier T, Hardy N, Harnly J, Higashi R, Kopka J, Lane AN,
1100 Lindon JC, Marriott P, Nicholls AW, Reily MD, Thaden JJ, Viant MR. 2007. Proposed
1101 minimum reporting standards for chemical analysis. Metabolomics 3:211-221.
1102 97. Gromski PS, Muhamadali H, Ellis DI, Xu Y, Correa E, Turner ML, Goodacre R. 2015. A
1103 tutorial review: Metabolomics and partial least squares-discriminant analysis - a
1104 marriage of convenience or a shotgun wedding. Analytica Chimica Acta 879:10-23.
1105 98. Haug K, Cochrane K, Nainala VC, Williams M, Chang J, Jayaseelan KV, O'Donovan C.
1106 2020. MetaboLights: a resource evolving in response to the needs of its scientific
1107 community. Nucleic Acids Res 48:D440-D444.
1108 99. Owens RA, O'Keeffe G, Smith EB, Dolan SK, Hammel S, Sheridan KJ, Fitzpatrick DA,
1109 Keane TM, Jones GW, Doyle S. 2015. Interplay between Gliotoxin Resistance,
1110 Secretion, and the Methyl/Methionine Cycle in *Aspergillus fumigatus*. Eukaryot Cell
1111 14:941-57.
1112 100. Sperling AS, Grunstein M. 2009. Histone H3 N-terminus regulates higher order
1113 structure of yeast heterochromatin. Proc Natl Acad Sci U S A 106:13153-9.
1114 101. Schindelin J, Arganda-Carreras I, Frise E, Kaynig V, Longair M, Pietzsch T, Preibisch S,
1115 Rueden C, Saalfeld S, Schmid B, Tinevez JY, White DJ, Hartenstein V, Eliceiri K,
1116 Tomancak P, Cardona A. 2012. Fiji: an open-source platform for biological-image
1117 analysis. Nature Methods 9:676-682.
1118 102. Mutterer J, Zinck E. 2013. Quick-and-clean article figures with FigureJ. Journal of
1119 Microscopy 252:89-91.
1120 103. Kavanagh K, Fallon JP. 2010. *Galleria mellonella* larvae as models for studying fungal
1121 virulence. Fungal Biol Rev 24:79-83.
1122 104. Gago S, Buitrago MJ, Clemons KV, Cuenca-Estrella M, Mirels LF, Stevens DA. 2014.
1123 Development and validation of a quantitative real-time PCR assay for the early
1124 diagnosis of coccidioidomycosis. Diagn Microbiol Infect Dis 79:214-21.
1125 105. Stajich JE, Harris T, Brunk BP, Brestelli J, Fischer S, Harb OS, Kissinger JC, Li W, Nayak V,
1126 Pinney DF, Stoeckert CJ, Jr., Roos DS. 2012. FungiDB: an integrated functional
1127 genomics database for fungi. Nucleic Acids Res 40:D675-81.
1128 106. Fiser A, Sali A. 2003. MODELLER: Generation and refinement of homology-based
1129 protein structure models. Macromolecular Crystallography, Pt D 374:461-491.

107. Alvarez-Carretero S, Pavlopoulou N, Adams J, Gilsenan J, Tabernero L. 2018. VSpipe, an Integrated Resource for Virtual Screening and Hit Selection: Applications to Protein Tyrosine Phospahatase Inhibition. Molecules 23.
108. Trott O, Olson AJ. 2010. Software News and Update AutoDock Vina: Improving the Speed and Accuracy of Docking with a New Scoring Function, Efficient Optimization, and Multithreading. Journal of Computational Chemistry 31:455-461.

1159 **FIGURE CAPTIONS**

1160 **Figure 1. Methionine synthase (MetH) enzymatic activity is essential for *A. fumigatus* viability.**

1161 **A)** Schematic representation of the trans-sulfuration pathway and its intersection with the one
1162 carbon metabolic route. **B)** Both strains, a *ΔmetF* mutant (which blocks the one carbon
1163 metabolism route) and a *ΔmetGΔcysD* mutant (which blocks the trans-sulfuration pathway)
1164 could grow in the presence of methionine. In contrast, the *metH_tetOFF* strain (*H_OFF*) could
1165 not grow in restrictive conditions (+Dox) even if methionine was supplemented. The phenotypic
1166 analysis was repeated in three independent experiments. Representative plates are shown. **C)**
1167 A second copy of the *metH* gene under the control of its own promoter was introduced in the
1168 innocuous *Ku70* locus of the *H_OFF* background strain. Two point-mutated versions of the gene
1169 were introduced, one that causes a D→A substitution in amino acid 616 and another one that
1170 causes a Y→A substitution in amino acid 662. In non-restrictive conditions all strains were able
1171 to grow as the parental *H_OFF* strain. In the presence of Dox and absence of met, the Y662A
1172 protein was able to trigger significant growth, suggesting that its enzymatic activity is impaired
1173 but not blocked. In the presence of Met the Y662A strain grew as well in restrictive as in non-
1174 restrictive conditions, suggesting that partial enzymatic activity is sufficient to cover the
1175 essential function of MetH. In restrictive conditions and absence of methionine, the D616A
1176 strain was not able to grow, indicating that enzymatic activity is blocked in this mutated protein.
1177 The D616A was also not able to grow in the presence of Dox and met, indicating that enzymatic
1178 activity is required for the essential function of MetH. The phenotypic analysis was repeated in
1179 three independent experiments. Representative plates are shown.

1180

1181 **Figure 2. Shortage of important downstream metabolites, but not toxic accumulation of**
1182 **homocysteine, partially accounts for MetH essentiality.**

1183 **A)** Supplementation of the growth media with a variety of downstream metabolites (Fig. 1A)
1184 showed that purines (adenine A and guanine G, 3 mM) could slightly reconstitute growth of the
1185 *H_OFF* strain in restrictive conditions. Further supplementation of amino acids improves growth,
1186 but not to the wild-type levels. Folic acid (5 mM) could also reconstitute growth when amino
1187 acids are the only N-source. **B)** Overexpression of genes that could detoxify a potential
1188 accumulation of homocysteine did not reconstitute growth in the absence of MetH activity.
1189 Further addition of adenine did not improve growth. The phenotypic analyses were repeated in
1190 three independent experiments. Representative plates are shown.

1191

1192 **Figure 3. Lack of methionine synthase activity causes a decrease in cell energetics.**

1193 **A)** Normalized concentrations of metabolites in fungal mycelia (*n*=8). Adenosine levels were
1194 decreased in *H_OFF*+Dox compared with *wt*+Dox, which agrees with its capacity to partially
1195 reconstitute growth. Several metabolites of the glycolysis and TCA pathways were reduced in
1196 *H_OFF*+Dox compared with *wt*+Dox, suggesting low energetic levels. **B)** The levels of ATP
1197 significantly decreased in the *H_OFF* strain upon Dox addition, whilst they did not vary
1198 significantly in the *wt* strain. Each point represents a biological replicate, which was assayed with
1199 three technical replicates. Data was analysed using one sample *t*-test to a hypothetical value of
1200 100 (i.e. no change in ratio of ATP). Graph displays the mean and standard deviation. **C)** Pyruvate
1201 as the sole carbon source could reconstitute growth of the *H_OFF* strain in restrictive conditions
1202 to wild-type levels. For both strains, growth was limited and slightly improved in the presence
1203 of amino acids. ATP could fully reconstitute growth of *H_OFF* when amino acids were the sole
1204 N-source. The phenotypic analyses were repeated in three independent experiments.
1205 Representative plates are shown. **D)** RT-PCR calculation of the fold-change in genetic expression
1206 of *metF* and *G6PD* with respect to their expression in wild-type without Dox. Each point
1207 represents a biological replicate which was analysed with three technical replicates. Data was
1208 analysed using one sample *t*-test to a hypothetical value of 1 (i.e. no change in expression).
1209 Graphs display the mean and standard deviation. **E)** Schematic representation of the metabolic
1210 imbalance started with MetH repression (1). Lack of the enzymatic activity caused a shortage of
1211 5,10-methylene-THF and consequently of purine rings (2). This was sensed as a shortage of
1212 nucleotides that the cell attempted to compensate through an unknown mechanism, seemingly
1213 TOR and PKA independent (3), that activated glucose flow through the Pentose Phosphate
1214 Pathway (PPP) (4). That caused a reduction of glycolysis and TCA cycles, which in turn decreased
1215 ATP levels (5). ATP usage for *S*-adenosylmethionine (SAM) synthesis was maintained, which
1216 caused a drop in cell energy that resulted in growth arrest (6). Genes/pathways/compounds
1217 expected to be reduced are highlighted in green and those increased in magenta.

1218

1219 **Figure 4. External *S*-adenosylmethionine (SAM) reconstitutes ATP levels and growth.**

1220 **A)** Addition of SAM to the medium reconstituted growth of the *H_OFF* strain in restrictive
1221 conditions. The phenotypic analysis was repeated in two independent experiments.
1222 Representative plates are shown. **B)** Levels of SAM did not significantly decrease upon Dox
1223 administration (5 µg/mL) in wild-type or *H_OFF* strains. Graphs depict mean and SD of three
1224 biological and two technical replicates. Data were analysed using one-way ANOVA with

1225 Bonferroni post-tests adjustment. **C)** Presence of SAM in the medium (0.5 mM) prevented the
1226 decrease in ATP levels observed in the *H_OFF* strain upon Dox addition. In fact, ATP levels were
1227 increased compared to the minus Dox condition. Graphs depict mean and SD of two biological
1228 and four technical replicates. **D)** Expression of MetH-GFP in the *H_OFF* background showed that
1229 the protein localised both in cytoplasm and nucleus. Singular channels are shown in greyscale.
1230 In composite image magenta=DAPI and green=GFP (Bar=10 µm).

1231

1232 **Figure 5. Repression of *metH* transcription causes inhibition of growth *in vitro.***

1233 **A)** Addition of 1 µg/mL Dox to 12 and 16 h grown mycelia strongly reduced fungal biomass,
1234 measured 24 h later. This was more pronounced in media without methionine. The effect was
1235 lost when Dox was added 24 h after inoculation. For comparison, fungal biomass of mycelia
1236 harvested at the time of Dox addition (12, 16 and 24 h post-inoculation) is shown. Three
1237 independent experiments were performed, using 3 technical replicates for each. **B)** Microscopic
1238 images of 8 h germinated spores treated with 10 µg/mL Dox. Images were taken 16 h after Dox
1239 addition (wide-field microscopy) and again 24 h later (stereomicroscopy). Dox addition halts
1240 growth of *H_OFF* strain in a sustained manner. **C)** Time-lapse microscopy of *H_OFF* growth upon
1241 Dox addition. Dox was added to 8 h grown conidia, which caused growth inhibition that was
1242 obvious after ~4 h. Growth was virtually halted for as long as Dox was present. **D)** ~6 h after Dox
1243 withdrawal, *H_OFF* growth resumed, showing that the effect was fungistatic.

1244

1245 **Figure 6. Downregulation of *metH in vivo* in established infections shows a beneficial effect**
1246 **comparable to the target of azoles.**

1247 **A)** Administration of a Dox regimen (Fig. S9A) to *Galleria mellonella* infected with either the
1248 *H_OFF* strain or the *51A_OFF* control strain showed a beneficial effect in survival. For both
1249 strains, starting regimen at the time of infection triggered a significant improvement in survival
1250 (50% VS 17.2% for *51A_OFF*, *P*=0.0036, and 41.45% VS 6.67% for *H_OFF*, *P*=0.022). Dox regimen
1251 6 h after infection also triggered a significant improvement in survival for both strains (42.8% VS
1252 17.2% for *51A_OFF*, *P*=0.0007, and 32.26% VS 6.67% for *H_OFF*, *P*=0.0324). The curves show the
1253 pooled data from 3 independent experiments. Curves were compared using the Log-Rank test.
1254 **B)** Leukopenic mice were infected with *51A_OFF* or *H_OFF* and a Dox regimen (Fig. S9B)
1255 administered 16 h after infection. Upon Dox treatment, fungal burden in the lungs was
1256 significantly reduced for both strains (*P*=0.0279 for *51A_OFF* and *P*=0.0019 for *H_OFF*). Two

1257 independent experiment were carried out. Each point in the graphs represents one mouse (n=9).
1258 Burdens for each strain were compared using a Mann Whitney test.

1259

1260 **Figure 7. Virtual-screening of fungal and human methionine synthases reveals different**
1261 **druggability of the proteins.**

1262 **A)** The structures of the crystallized *C. albicans* and the predicted A. *fumigatus* methionine
1263 synthases are highly similar. **B)** In contrast, the structure of the human enzyme is very different,
1264 having he 5-methyl-tetrahydrafolate and homocysteine binding sites separated. **C)** Detail of the
1265 active site of fungal methionine synthases, with the methionine, folate and zinc displayed. **D)**
1266 Tetrahydrofolate binding site of the human protein. **E)** Virtual screening on the *A. fumigatus*
1267 protein found four ligand binding clusters in the structure, two of which (C1, C2) match the
1268 binding position of the 5-methyl-tetrahydrafolate and the methionine. **F)** In the human enzyme
1269 two clusters were found, one (C1) that overlaps with the tetrahydrofolate binding site and
1270 (another C2) in a nearby pocket.

1271

1272

1273

1274

1275

1276

1277

1278

1279

1280

1281

1282

1283

1284

1285

1286 **SUPPLEMENTARY FIGURES**

1287 **Figure S1.**

1288 **A)** Addition of 1 µg/mL Dox to a 16 h growing mycelia quickly downregulated transcription of
1289 *metH*. **B)** The growth of two *metH_tetOFF* strains in two different backgrounds was prevented
1290 in the presence of as little as 0.5 µg/mL Dox, even in the presence of methionine. The phenotypic
1291 analysis was repeated in three independent experiments. Representative plates are shown. **C)**
1292 An *A. fumigatus ΔmetGΔcysD* mutant (methionine auxotroph) was completely avirulent in a
1293 leukopenic murine model of invasive pulmonary aspergillosis. **D)** A strain expressing a C-
1294 terminus-GFP-tagged MetH-D616 protein from the pJA49 overexpression plasmid (Fig. S2) in the
1295 *H_OFF* background strain showed fluorescence in -Dox conditions (did not grow in +Dox
1296 conditions, Fig. S5), proving that the point mutated MetH-D616 protein is stable.

1297 **Figure S2.**

1298 **A)** Schematic representation of the pJA49 plasmid for episomal overexpression of genes in *A.*
1299 *fumigatus*. It carries the *A. nidulans* AMA1 autologous replicating sequence and the hygromycin
1300 B resistance gene (*hygrB*) as a selection marker. A unique *Stu*I restriction site allows introduction
1301 of any PCR amplified ORF in frame under the control of the *A. fumigatus* strong promoter *hspA*
1302 and the *A. nidulans trpC* terminator. **B)** Schematic representation of the genes overexpressed
1303 (in green) to eliminate potential accumulation of toxic homocysteine and derivatives (in red). **C)**
1304 Fold change in expression level of *mecA* and *sahL* measured by RT-PCR. Both genes are highly
1305 overexpressed from plasmid pJA49. **D)** Expression level of *blhA* determined by retrotranscription
1306 and PCR (fold change cannot be calculated as this gene is not expressed in *A. fumigatus*).

1307 **Figure S3.**

1308 Relevance of the nitrogen source for the capacity of different metabolites to reconstitute growth
1309 of the *H_OFF* strain in restrictive conditions. Amino acids alone were not able to reconstitute
1310 growth. Folic acid could partially, and ATP and SAM completely reconstituted growth when
1311 amino acids were the only N-source, suggesting that they are only taken up when there is a high
1312 variety of permeases in the cell membrane. Pyruvate could reconstitute growth to wild-type
1313 level in the absence of glucose and independently of the in presence of amino acids, although
1314 growth improved when they were added.

1315 **Figure S4.**

1316 **A)** Principal component analysis (PCA) scores plot of the GC-MS metabolome analysis. The wild-
1317 type and *H_OFF* strains clusters were close before addition of Dox and became clearly separated

1318 upon 6 h incubation in the presence of Dox. **B)** The content of several amino acids and sugars
1319 were reduced in the H_OFF+Dox sample compared with the developmentally matched wt+Dox
1320 sample. **C)** Neither low concentrations of rapamycin (to partially inhibit TOR) nor of H89 (to
1321 partially inhibit PKA) were able to reconstitute growth of the *H_OFF* strain in restrictive
1322 conditions. This suggests that these regulatory pathways are not responsible for the deleterious
1323 switch in metabolism that causes a drop in cellular ATP.

1324 **Figure S5.**

1325 **A)** Expression of MetH-GFP wild type and $MetH^{R742A}$-GFP reconstituted growth of the *H_OFF*
1326 strain in restrictive conditions, demonstrating that the proteins are active. As expected, the
1327 inactive protein $MetH^{D616A}$-GFP did not trigger growth. **B)** Western-blot of MetH. Strains
1328 expressing MetH-GFP wild type and $MetH^{R742A}$-GFP were grown in the presence of Dox, nuclei
1329 isolated from the mycelia (as described in material and methods), proteins purified and blotted
1330 with an anti-GFP antibody. The $MetH^{R742A}$-GFP protein could be detected in nuclei, at similar
1331 levels as the wild-type MetH-GFP.

1332 **Figure S6.**

1333 Doxycycline can perturb *A. fumigatus* hyphal mitochondrial morphology at high concentrations.
1334 *A. fumigatus* hyphae were stained with 10 µM Rhodamine 123 after overnight incubation in **A)**
1335 0 µg/ml, **B)** 1000 µg/ml, **C)** 1 µg/ml, **D)** 10 µg/ml and **E)** 100 µg/ml Doxycycline. Representative
1336 single plane confocal fluorescence images are displayed in A-E. Notice the granulation in B (1000
1337 µg/ml and variable response in E (100 µg/ml), whereas C (1 µg/ml) and D (10 µg/ml) display
1338 normal mitochondrial morphology . Scale bars = 10 µm.

1339 **Figure S7.**

1340 **A)** Measurement of fungal growth by Optical Density (OD) showed that addition of 1 µg/mL Dox
1341 12 or 16 h after inoculation significantly reduced fugal growth at 24 and 36 h post-incubation.
1342 **B)** Microscopy analysis of the effect of the addition of 2 concentrations of Dox to resting or 8 h
1343 germinated conidia of the *H_OFF* strain. In the absence of methionine growth is immediately
1344 halted in a sustained manner. In the presence of methionine conidia can germinate and
1345 germlings elongate the growing tube before growth stops. However, once arrested, growth is
1346 halted in a sustained manner. Microimages were taken with a wide-field microscope at 16 h
1347 post-inoculation and with a stereomicroscope 40 h after inoculation (to be able to capture the
1348 huge mass of fungal growth in the control conditions).

1349 **Figure S8.**

1350 **A)** Colony formation of the strain *cyp51A_tetOFFΔcyp51B* (*51A_OFF*) is completely prevented
1351 with as little as 0.1 µg/mL on an agar plate. Phenotypic analysis was repeated in two
1352 independent experiments. **B)** Microscopy analysis of the effect of the addition of 2
1353 concentrations of Dox to resting or 8 h germinated conidia of the 51A_*OFF* strain. In both cases
1354 growth is immediately blocked. We could observe bursting germlings with high doses of Dox
1355 (red arrow).

1356 **Figure S9.**

1357 **A)** Dox regime applied to *Galleria mellonella*. A maximum of 5 doses (50 mg/kg) were applied,
1358 commencing either at the time of infection or 6 h later. **B)** Dox regimen administered to mice.
1359 Treatment started 16 h after infection with a subcutaneous (SC) Dox injection (50 mg/kg) and
1360 change to Dox food. Treatment was maintained with SC injections every 12 h after the infection
1361 time-point. Dox concentration in the lungs was measured in a preliminary experiment with
1362 uninfected mice. Lungs were harvested 4 h after the beginning of treatment, 2 h after the third
1363 injection (on day 2) and 9 h after the 5th (on day 3, last injection). The concentrations were
1364 determined to range from 0.9 to 2.2 µg/mL, sufficient to downregulate gene expression
1365 according to the results *in vitro*.

1366 **Video S1**

1367 Time-lapse of growth of the *H_OFF* strain upon Dox addition and withdrawal.

1368 **Video S2**

1369 Time-lapse of growth of the *wild-type* strains upon Dox addition.

Fig. 1

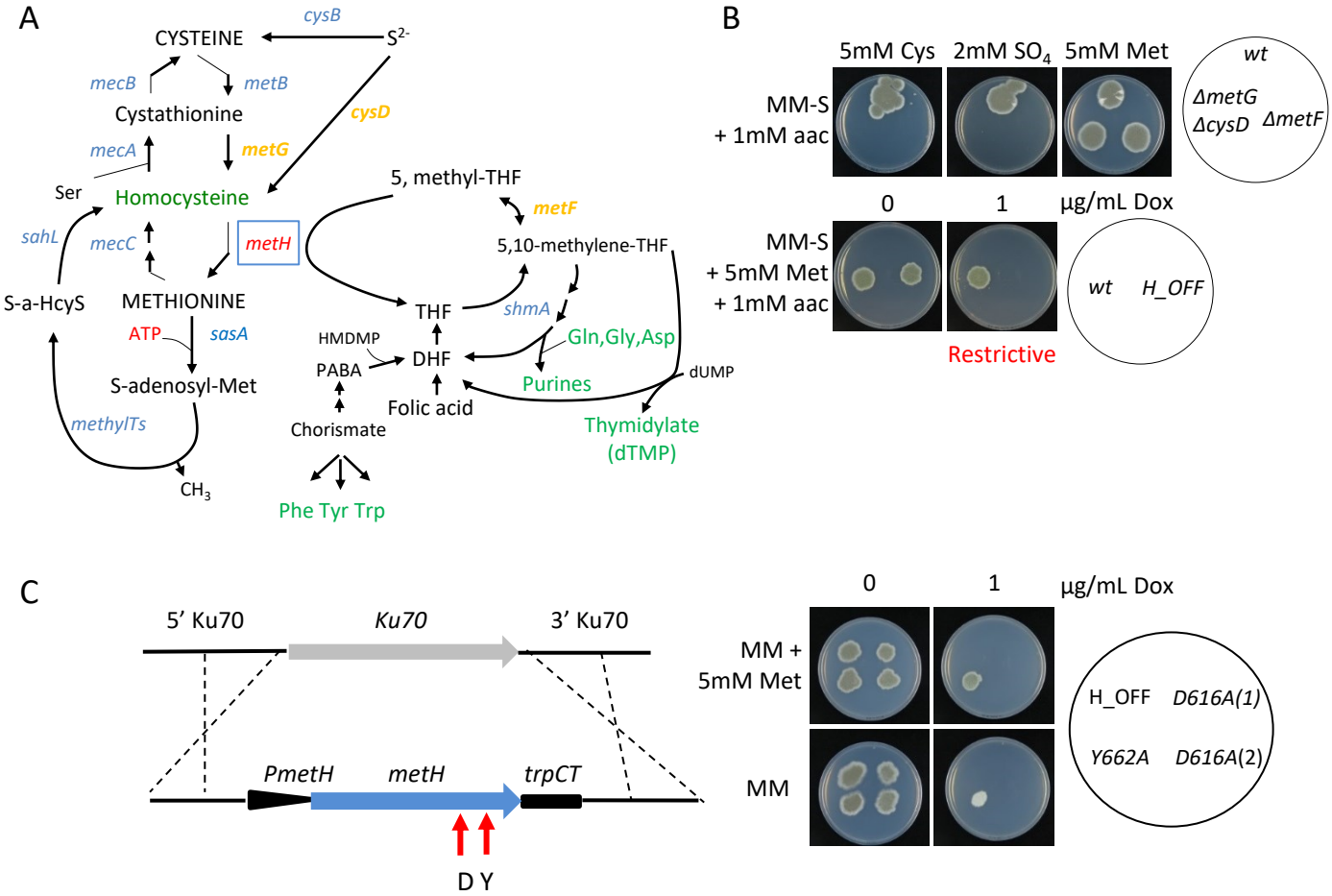
A
CYSTEINE
cysB
S2-
mecB
metB
Cystathionine
cysD
mecA
metG
Ser
Homocysteine
5, methyl-THF
metF
sahL
mecC
metH
5,10-methylene-THF
S-a-HcyS
METHIONINE
THF
shmA
ATP
sasA
HMDMP
Gln,Gly,Asp
PABA
DHF
S-adenosyl-Met
Purines
dUMP
Folic acid
methylTs
Chorismate
Thymidylate
(dTMP)
CH3
Phe Tyr Trp
B
5mM Cys
2mM SO4
5mM Met
MM-S
+ 1mM aac
wt
ΔmetG
ΔcysD
ΔmetF
0
1
µg/mL Dox
MM-S
+ 5mM Met
+ 1mM aac
wt
H_OFF
Restrictive
C
5' Ku70
Ku70
3' Ku70
PmetH
metH
trpCT
D Y
0
1
µg/mL Dox
MM +
5mM Met
MM
H_OFF
D616A(1)
Y662A
D616A(2)

Fig. 2

A

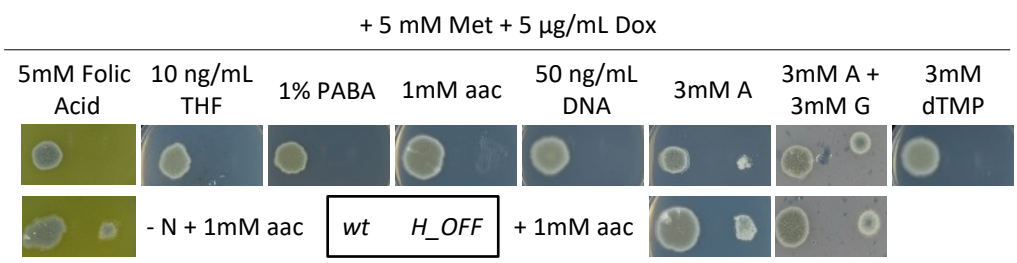
+ 5 mM Met + 5 µg/mL Dox
5mM Folic Acid
10 ng/mL THF
1% PABA
1mM aac
50 ng/mL DNA
3mM A
3mM A + 3mM G
3mM dTMP
- N + 1mM aac
wt
H_OFF
+ 1mM aac

B

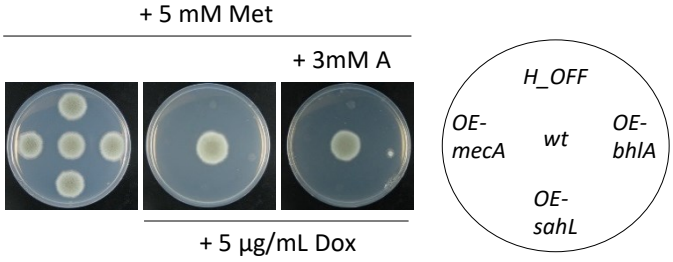
+ 5 mM Met
+ 3mM A
+ 5 µg/mL Dox
H_OFF
OE-mecA
wt
OE-bhlA
OE-sahL

Fig. 3

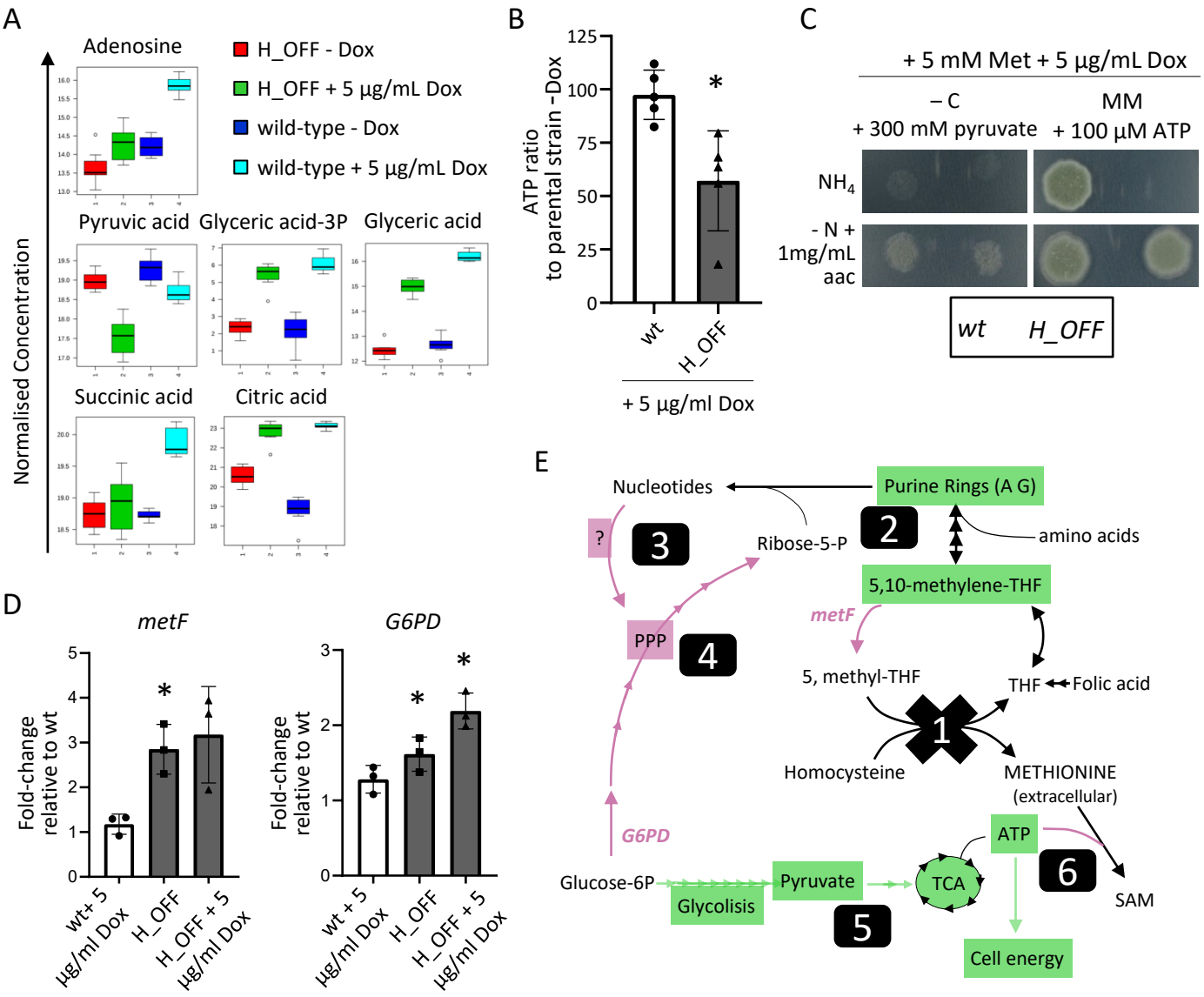
A
Adenosine
H_OFF - Dox
H_OFF + 5 µg/mL Dox
wild-type - Dox
wild-type + 5 µg/mL Dox
Pyruvic acid
Glyceric acid-3P
Glyceric acid
Succinic acid
Citric acid
Normalised Concentration
B
ATP ratio to parental strain -Dox
wt
H_OFF
+ 5 µg/ml Dox
C
+ 5 mM Met + 5 µg/mL Dox
– C
+ 300 mM pyruvate
MM
+ 100 µM ATP
NH4
- N + 1mg/mL aac
wt
H_OFF
D
metF
G6PD
Fold-change relative to wt
wt+ 5 µg/ml Dox
H_OFF
H_OFF + 5 µg/ml Dox
E
Nucleotides
Purine Rings (A G)
Ribose-5-P
amino acids
5,10-methylene-THF
metF
PPP
5, methyl-THF
THF
Folic acid
Homocysteine
METHIONINE (extracellular)
ATP
G6PD
Glucose-6P
Glycolisis
Pyruvate
TCA
SAM
Cell energy

Fig. 4

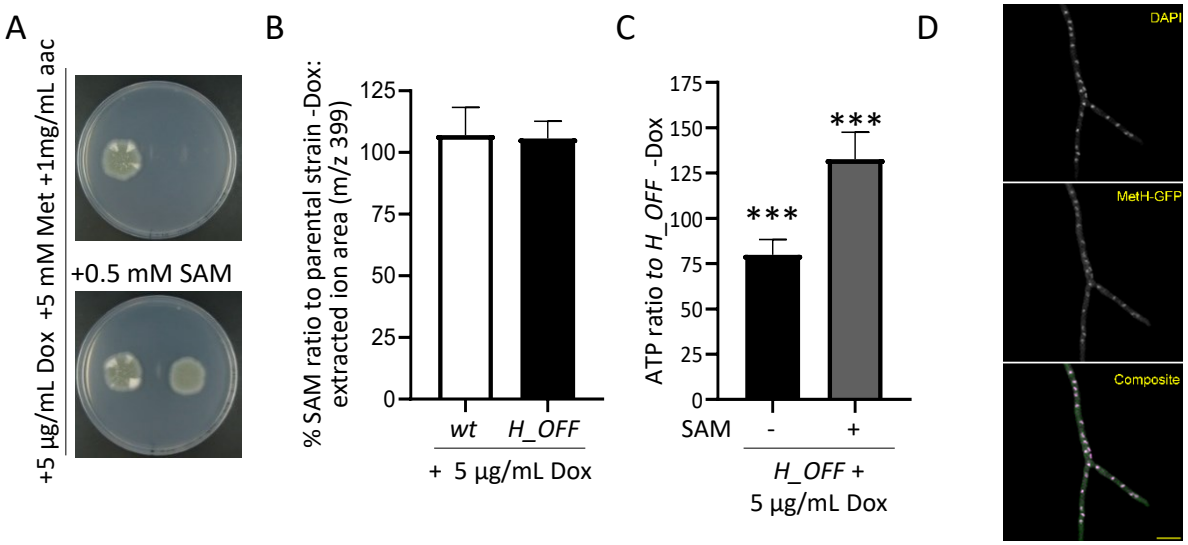
A
+5 µg/mL Dox +5 mM Met +1mg/mL aac
+0.5 mM SAM
B
% SAM ratio to parental strain -Dox: extracted ion area (m/z 399)
125
100
75
50
25
0
wt
H_OFF
+ 5 µg/mL Dox
C
ATP ratio to H_OFF -Dox
175
150
125
100
75
50
25
0
***
***
SAM
-
+
H_OFF +
5 µg/mL Dox
D
DAPI
MetH-GFP
Composite

Fig. 5

A

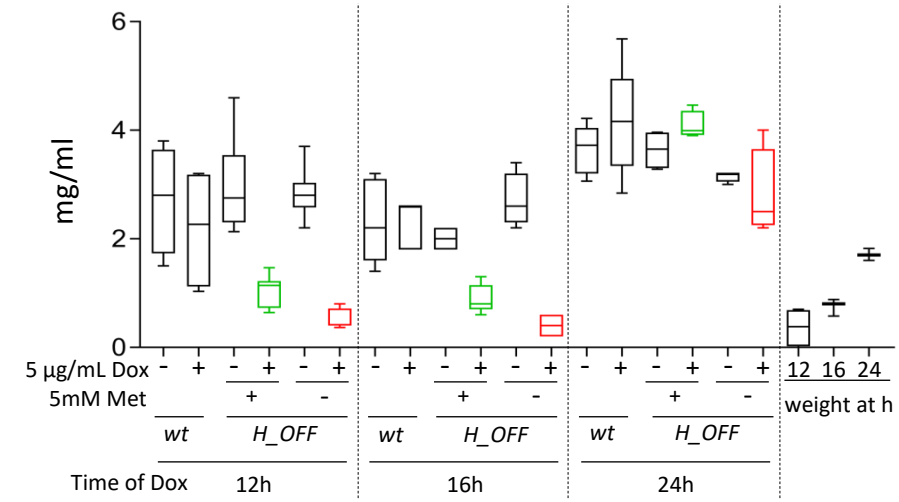
mg/ml
6
4
2
0
5 µg/mL Dox
5mM Met
wt
H_OFF
Time of Dox
12h
16h
24h
12 16 24
weight at h

B

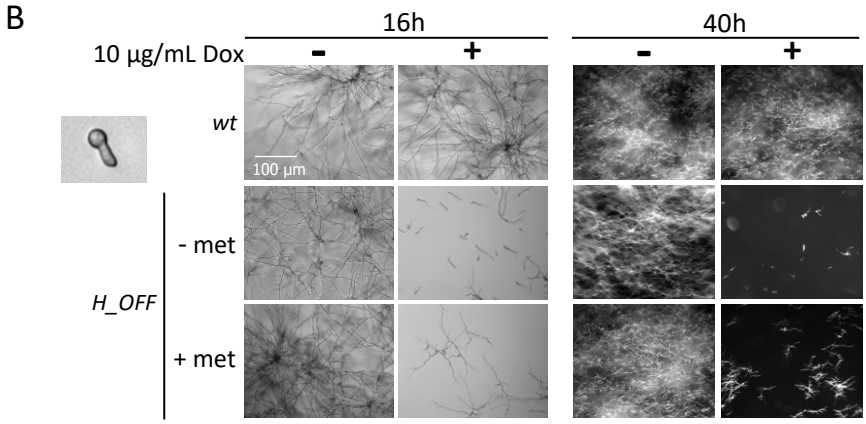
16h
40h
10 µg/mL Dox
-
+
wt
100 µm
H_OFF
- met
+ met

C

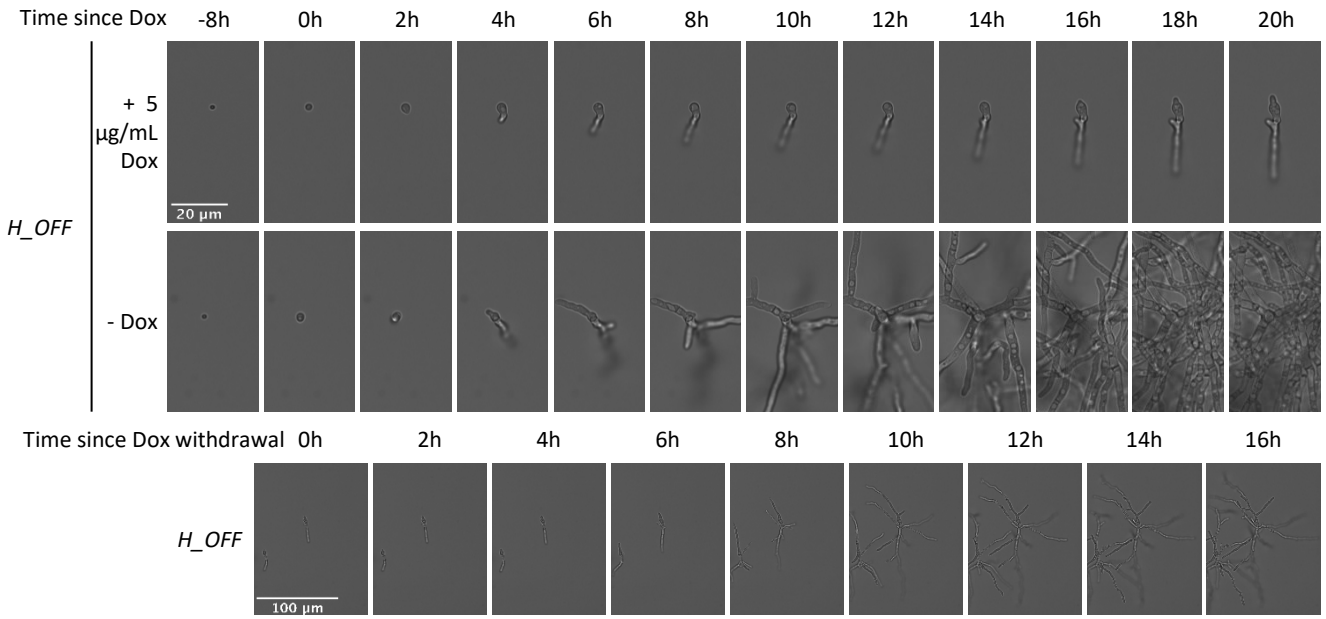
Time since Dox
-8h
0h
2h
4h
6h
8h
10h
12h
14h
16h
18h
20h
+ 5 µg/mL Dox
- Dox
H_OFF
20 µm
Time since Dox withdrawal
0h
2h
4h
6h
8h
10h
12h
14h
16h
H_OFF
100 µm

Fig. 6

A

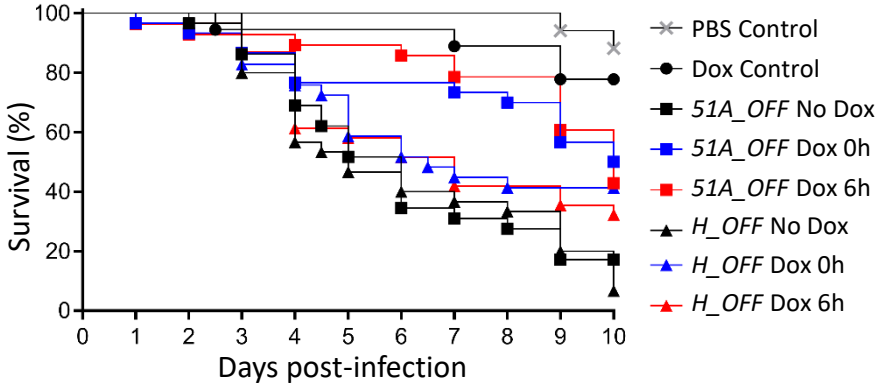
Survival (%)
100
80
60
40
20
0
0
1
2
3
4
5
6
7
8
9
10
Days post-infection
PBS Control
Dox Control
51A_OFF No Dox
51A_OFF Dox 0h
51A_OFF Dox 6h
H_OFF No Dox
H_OFF Dox 0h
H_OFF Dox 6h

B

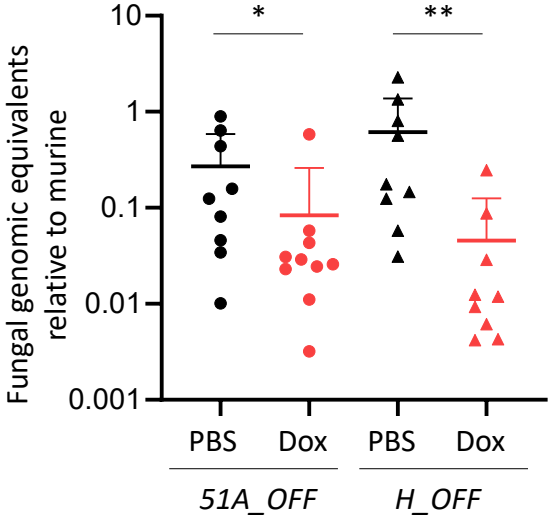
Fungal genomic equivalents relative to murine
10
1
0.1
0.01
0.001
*
**
PBS
Dox
PBS
Dox
51A_OFF
H_OFF

Fig. 7

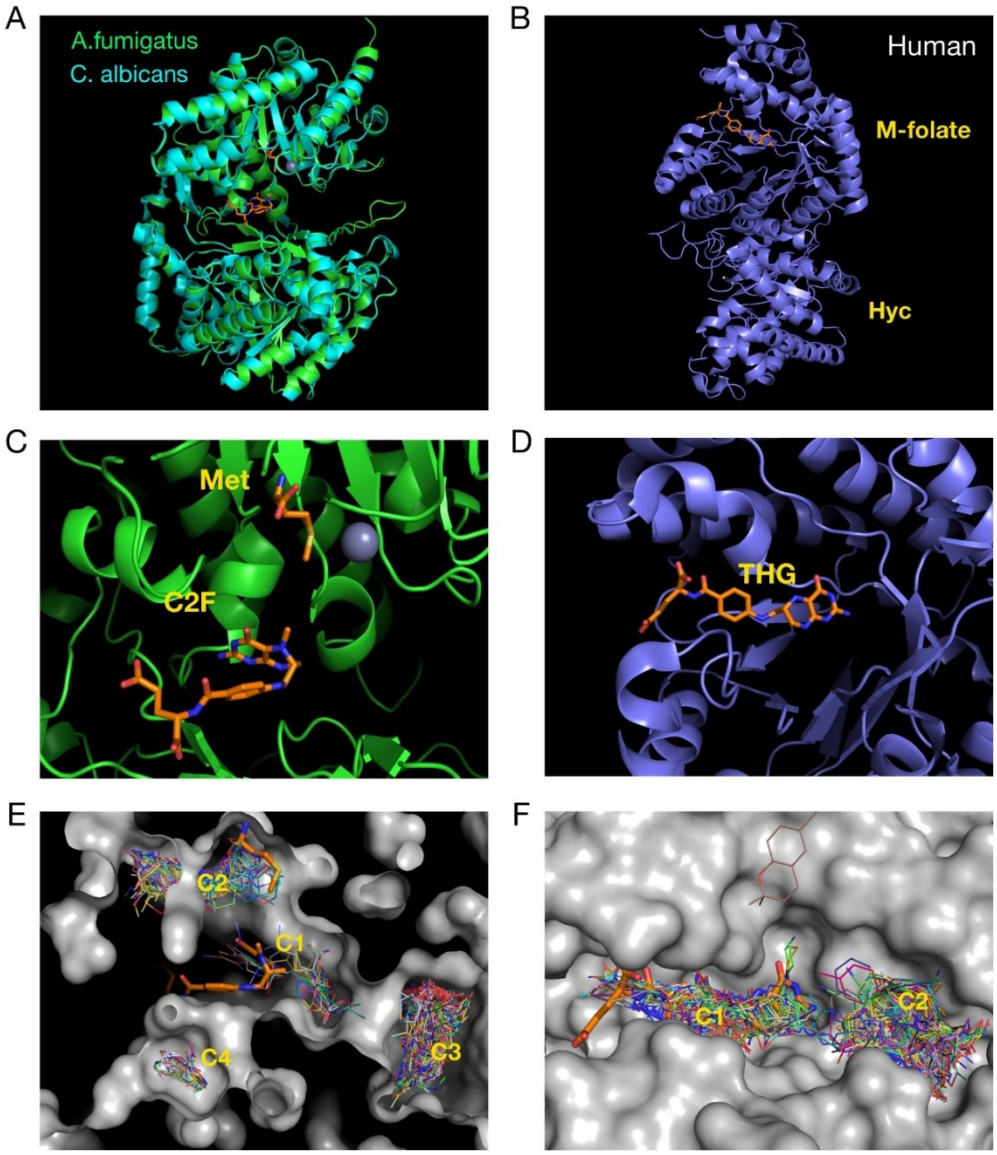
A
A.fumigatus
C. albicans
B
Human
M-folate
Hyc
C
Met
C2F
D
THG
E
C2
C1
C4
C3
F
C1
C2